

Green Chemistry Letters and Reviews



ISSN: 1751-8253 (Print) 1751-7192 (Online) Journal homepage: http://www.tandfonline.com/loi/tgcl20

A peony-leaves-derived liquid corrosion inhibitor: protecting carbon steel from NaCl

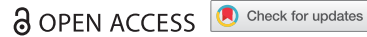
Mehdi Honarvar Nazari, Mehdi Salih Shihab, Ling Cao, Eden Adele Havens & Xianming Shi

To cite this article: Mehdi Honarvar Nazari, Mehdi Salih Shihab, Ling Cao, Eden Adele Havens & Xianming Shi (2017) A peony-leaves-derived liquid corrosion inhibitor: protecting carbon steel from NaCl, Green Chemistry Letters and Reviews, 10:4, 359-379, DOI: 10.1080/17518253.2017.1388446

To link to this article: https://doi.org/10.1080/17518253.2017.1388446

9	© 2017 The Author(s). Published by Informa UK Limited, trading as Taylor & Francis Group
	Published online: 27 Oct 2017.
Ø	Submit your article to this journal 🗷
ılıl	Article views: 481
CrossMark	View Crossmark data 🗗







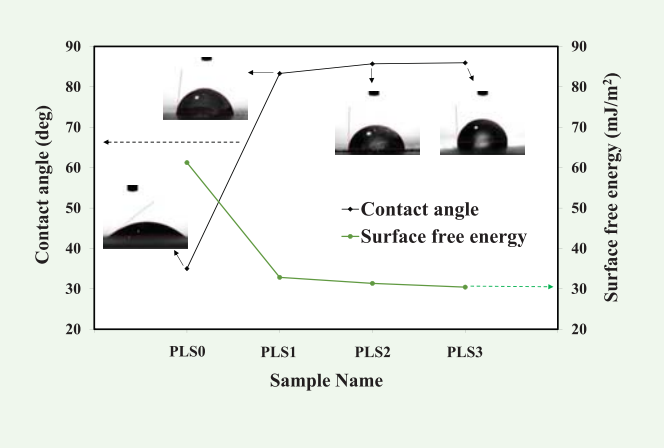
A peony-leaves-derived liquid corrosion inhibitor: protecting carbon steel from **NaCl**

Mehdi Honarvar Nazari^a, Mehdi Salih Shihab^b, Ling Cao^c, Eden Adele Havens^a and Xianming Shi oa

^aLaboratory of Corrosion Science & Electrochemical Engineering, Department of Civil & Environmental Engineering, Washington State University, Pullman, WA, USA; Department of Chemistry, College of Science, Al-Nahrain University, Baghdad, Iraq; Western Transportation Institute, College of Engineering, Montana State University, Bozeman, Montana, USA

ABSTRACT

A liquid mixture was developed from waste peony leaves through a zero-waste chemical/biological process. The inhibition effect of different concentrations of peony leaves derived solution (0-3 vol.%, PLS0-3) on C1010 carbon steel in 3.5 wt.% NaCl was investigated over time using electrochemical measurements. Chemical analyses were performed to reveal the main compounds of this inhibitor. Surface analyses together with water contact angle measurements were employed to study the characteristics of the steel surface affected. Semi-empirical calculations with PM3 method were used to find the relationship between molecular structure and inhibiting effect of PLS. The inhibitor was stable over time and its main active ingredients were $C_{19}H_{27}N_4O_{10}P$ and $C_{17}H_{16}N_3O_9P$ that adsorb onto the steel surface, block cathodic active sites, make the surface hydrophobic, decrease the surface free energy, and facilitate the formation of a passive layer. A good correlation was found between experimentally determined inhibition efficiency and theoretically calculated properties of PLS.



ARTICLE HISTORY

Received 20 March 2017 Accepted 2 October 2017

KEYWORDS

Corrosion inhibitor; carbon steel; IR spectroscopy; EIS; passive film

1. Introduction

Chlorides are the most common freezing point depressants found in road salts (a.k.a., deicers), which induce significant environmental footprint while providing benefits to society and traveling public (1-3). In the U.S. alone, about 20 million tons of chloride-based salts are used annually to keep roadways free of snow and ice (4). These salts are highly soluble, very mobile, difficult to remove, and inherently corrosive. They may pose shortterm and long-term risks to water (5-8), soil (9), vegetation (10), wildlife (11), and transportation assets (12). For instance, Siegel tested toxicity thresholds of chloride for 21 aquatic species and found fathead minnow being the most sensitive species with an acute toxicity level of 874 mg Cl⁻/L and chronic exposure of 252 mg Cl⁻/L (13).

Corrosion of transportation infrastructure and motor vehicles can also induce significant environmental footprint, due to the increased need of maintenance and repair activities, associated traffic congestion, and the release of metallic elements caused by corrosion. For instance, iron which is the main component of steels can pose toxicological risk toward aquatic species (14, 15). It can also complex with toxic substances and increase their toxicity. A recent study reveals that Fe(III)

may induce oxidation of antibiotics in water, causing a stronger toxicity than parent antibiotics (16). Zinc is another metal of concern due to its bioavailability and toxicity to aquatic species such as early-life-stage white sturgeon (17), and it is commonly used in galvanized steels seen in motor vehicles and guardrails.

Corrosion inhibitors are proven to be effective in reducing the metallic corrosion and thus preserving the service life and performance of assets (18). Furthermore, a recent study revealed that some agro-based inhibitors can offer additional benefits as "cryoprotectants," i.e., significantly lowering the freezing point of salt brine (19), which may translate to reduced salt application rates needed under cold weather scenarios. In place of petroleum-derived inhibitors, inhibitors from renewable resources (a.k.a., green inhibitors) are highly desirable as they are less toxic, readily available and bio-degradable, and more cost-effective (20-22).

Plant extracts have been disclosed to contain effective, user-friendly, and environmentally friendly ingredients for corrosion inhibition (20, 21, 23–25). Such green inhibitors feature organic compounds containing heteroatoms such as P, S, N, and O which can adsorb onto the metallic surface and form a protective layer (23–27). The adsorption of these polar atoms is made possible by the co-ordination between their non-bonded (lone pair) or π -electron cloud and the metal surface. This is known as chemical adsorption or adsorption due to electrostatic interaction between the organic molecules and the metallic surface (26, 28–31). The inhibition efficiency of these polar atoms usually obeys the following sequence (28):

$$P > S > N > O. \tag{1}$$

Many plant extracts have been studied for their potential as green corrosion inhibitors for carbon steel in NaCl solution. The most updated articles have used Theobroma cacao (32), Kudingcha (33), Origanum majorana (34), Morinda citrifolia (35), Neem leave (36), and Myrmecodia pendans (37). Yetri et al. (32) evaluated the corrosion inhibition behavior of T. cacao peels extract on mild steel in 1.5 M NaCl. The inhibition efficiency increased with increasing the concentration of extract with a maximum efficiency of 91.93% at 2.5 vol.% of extract, based on weight loss test. The efficiency decreased slightly with increasing the temperature. The extract contained phenolic and alkaloid compounds as main components and there was chemical bonding between the extract molecules and the steel surface. The inhibitor obeyed Langmuir isotherm adsorption and acted as mixed inhibitor with dominant cathodic inhibition. Chen et al. (33) evaluated Kudingcha C.J. Tseng extract as a green inhibitor for J55 steel in 3.5 wt.% NaCl solution. They tested 0-4 vol.% of the

extract and found that this extract has its best corrosion inhibition efficiency (92.65%) at 4 vol.% based on polarization curves. Kudingcha extract behaved as a mixed type of inhibitor and adsorbed onto the steel surface following the Langmuir isotherm. Challouf et al. (34) used O. majorana extract as a green inhibitor for mild steel in 0.5 M NaCl solution. They optimized the extraction parameters using chemiometric approach method and reached 90% inhibition efficiency according to the polarization curves (the concentration of inhibitor was not given in the manuscript). An increase in the activation energy was observed in the presence of the O. majorana extract that could be related to the physical adsorption process. Based on thermodynamic adsorption parameters the extract adsorbed on the surface of steel by an exothermic process. The molecule responsible for the inhibition action was determined using quantum chemical calculations. Kusumastuti et al. (35) evaluated M. citrifolia as a green corrosion inhibitor for mild steel in 3.5% NaCl solution. The inhibition efficiency reached its maximum (68.08%) at 3 ppm, based on polarization curves, and then decreased in the presence of further inhibitor. The adsorption isotherm followed the Langmuir adsorption model and showed the behavior of a mixed type inhibitor that formed a monolayer protective film. Tuaweri et al. (36) used Neem leave extract as a corrosion inhibitor for mild steel in natural sea water. The corrosion rate was least with 5 vol.% extract and increased with increase in extract concentration based on weight loss test. Pradityana et al. (37) used M. pendans extract as a green corrosion inhibitor for carbon steel in 3.5% NaCl Solution. The highest inhibition efficiency occurred in the presence of 400 mg/L extract. The mechanism of inhibition was formation of a protective film due to the adsorption of extract molecules onto the metal surface, following the Langmuir isotherm. This film was formed from complex compounds, supported by new bonds such as Fe-N-H and Fe-O.

This work explores an innovative process to derive green inhibitor from waste peony leaves, consisting of rapid dissolution of the leaves (chemical degradation) followed by biological degradation. This is the first effort to derive corrosion inhibitor from peony leaves. In the State of Alaska alone, there are 58 peony farms that can produce about 200,000 peonies annually (38), which after the flower season generate a substantial amount of peony leaves as waste. The up-cycling of this waste can benefit the environment and the economy. The use of urea for dissolution of flower leaves in alkaline solution is a new method, which has been previously reported to fabricate fibers from cellulose (39). Furthermore, this is the first report of a process of deriving corrosion inhibitor from plants, enabled by the biological approach. Usually



only chemical approach has been adopted for deriving corrosion inhibitors from plants, using methanol (40, 41), ethanol (23, 24, 27), water (42, 43), hexane (44), and other solvents, which often still produce liquid waste from the process.

In this laboratory study, the corrosion inhibition performance and mechanism of peony leaves derived solution were investigated using C1010 carbon steel coupons continuously immersed in 3.5 wt.% NaCl solutions over 16 days. Methods employed include chemical analyses, electrochemical measurements, surface analyses, and water contact angle measurement. The findings will contribute to the search for a sustainable approach to mitigating the environmental impacts of chlorides and steel corrosion.

2. Experimental procedure

2.1. Materials

Test coupons were made of C1010 carbon steel purchased with the nominal composition shown in Table 1. To fabricate the coupons, the material was cut from larger sheets into small size of about 1 cm × 1 cm. The unexposed side of each coupon was then electrically connected to a copper wire by soldering, followed by sealing with marine epoxy resin (Hawk Epoxy R1 Resin). After the curing of the epoxy sealer, the coupons were polished to provide a specific level of uniform surface roughness. They were wet-polished using 60-1500 grit silicon carbide papers, respectively. After polishing at each grit size, the coupons were rinsed with running tap water to remove any remaining grit. The last step was washing the coupons by deionized water and then cleaning with a clean paper tissue.

The experiments were carried out in a glass cell filled with 120 mL of simulated seawater (3.5% NaCl, which is known to be a highly corrosive concentration) at atmospheric pressure and room temperature for 16 days (384 h). Three concentrations of peony leaves derived solution as 1.0, 2.0, and 3.0 vol.% were used. For reproducibility of the results from each experiment, at least two duplicate coupons were used. The code names of brine and steel samples are provided in Table 2.

For preparation of the liquid extract, the peony leaves were collected from Alaska, U.S.A, dried, frozen, and then milled into powder. Thirty grams of this powder was

Table 1. Chemical composition of C1010 steel.

		Elen	nent (wt.%)		
Alloy	С	Mn	Р	S	Fe
C1010	0.08-0.13	0.30-0.60	≤0.04	≤0.05	Balance

Table 2. The code names of brine and steel samples used in this research.

Definition	Coupons immersed in 3.5 wt.% NaCl with different concentrations of peony leaves derived solution (green inhibitor)				
Inhibitor concentration (vol.%)	0	1	2	3	
Sample	PLS0	PLS1	PLS2	PLS3	

chosen for further degradation. For chemical degradation of the leaves, 120 g urea and 0.5 g Ca(OH)₂ were added to 200 mL deionized water. Then the aforementioned powder was added to this solution, and 4 g NaOH was subsequently added to obtain a solution pH of 11.6. This solution was stirred at the speed of 500 rpm for 30 min and then placed in the refrigerator at -13°C. Once the freezing process started, the solution was brought out and 500 mL deionized water was slowly added into it with simultaneous stirring at 150 rpm for 30 min. This is followed by the biological degradation procedure: first, the pH of prepared solution was adjusted to 8.5 by adding $15\,\mathrm{mL}$ HNO₃ and $6.5\,\mathrm{g}$ NaOH. Then, a mixture of 1.274 g KH₂PO₄, 1.952 g NaH₂-PO₄·H₂O, and 0.182 g MgSO₄·7H₂O was added to the solution to create a medium suitable for the growth of bacteria. Next, 100 mL of Bacillus Megaterium bacteria (NRRL B-14308) was added to the solution, which was subsequently placed in a shaker for 14 days. Finally, the resulting mixture was used as the corrosion inhibitor without further treatment or purification. For studying the effect of peony leaves on the behavior of solution, a solution without peony leaves (SWPL) according to the above-mentioned process was prepared. Note that all the chemicals used in this work were of analytical grade purity and purchased from J.T. Baker or Sigma-Aldrich and the aforementioned process has been protected by a patent application.

2.2. Chemical analyses

The chemical functional groups of the dried peony leaves extract were studied using Fourier transformed - infrared (FT-IR) spectroscopy technique via a Nicolet 6700 FT-IR Spectrometer (Thermo Fisher Scientific, Madison, WI). The IR spectra of the samples were collected over the wave number range of 4000–400 cm⁻¹.

Detection of metabolites in the peony leaves liquid extract was performed via liquid chromatography-mass spectrometry (LC-MS) technique. First, the extracts were diluted 1:1 with methanol, then the debris was removed by centrifugation for 10 min, and the resulting supernatant was filtered through a 0.2-µm Acrodisc filter. Of the resulting extracts, 2 μ L were loaded onto a 50 \times 2.1 mm Acquity BEH C18 column (Waters) and eluted



using a linear gradient of acetonitrile-water containing 0.1% formic acid at a flow rate of 0.4 mL/min. The analysis was conducted in positive ion mode using Synapt G2-S (Waters), a quadrupole time-of-flight mass spectrometer. The capillary was at 3 kV, the source temperature at 120°C, desolvation gas flow at 850 L/h. The data collected were corrected using the signal of the coinfused reference compound leucine enkephalin.

2.3. Electrochemical measurements

The electrochemical tests were carried out using a threeelectrode cell and a PARSTAT MC multichannel Potentiostat, with Ag/AgCl as reference electrode and platinum mesh as counter electrode. The linear polarization resistance (LPR) measurements were periodically conducted by polarizing the steel coupon (working electrode) ±20 mV vs. the open-circuit potential (OCP) at a rate of 0.167 mV/s. The electrochemical impedance spectroscopy (EIS) measurements were conducted in a frequency range of 100 kHz to 0.005 Hz with an applied alternating current (AC) signal of ±10 mV around the OCP. Potentiodynamic polarization (PDP) tests were carried out at a potential sweep rate of 0.167 mV/s in the range of -250 mV to +400 mV relative to OCP. The VersaStudio software was employed to perform all of the electrochemical measurements. The interpretation of the EIS data was performed using the ZSimpWin 3.60 software.

2.4. Surface analyses

The phase analysis of corrosion product scale was conducted via the grazing incidence X-ray diffraction (GIXD) method with a SCINTAG X1 diffraction system using Cu-Ka radiation. GIXRD is a very useful technique for investigating thin films (45). The morphology of the corrosion product layers was studied via a field emission scanning microscopy (FESEM) instrumentation model Zeiss SUPRA 55VP coupled with the energy dispersive X-ray analyzer. For in-depth investigation of corrosion product layers in the presence of green inhibitor, the X-ray photoelectron spectroscopy (XPS) analysis was conducted on a Physical Electronics 5600ci XPS system equipped with monochromatized Al K alpha X-rays. The analysis area of the steel samples was 0.8 mm in diameter. Electron emissions were collected at 45 degrees to the normal surface, and the sphericalsector-analyzer pass energy was selected as 23.45 eV for high resolution and 46.95 eV for a survey to achieve optimum energy resolution and count rate. The data acquisition and data analysis were performed using the RBD AugerScan 3 software.

2.5. Contact angle measurement

Hydrophilicity of the steel coupons was assessed by measuring the contact angle between a water drop and the steel surface using a VCA-2500XE contact angle system (ASC products). The drops of nanopore water were mounted on the surface of carbon steel sample using a micro-syringe with needle diameter of 0.4 mm. The reported contact angles were an average of at least three measurements on different areas of the surface. Photos of water drops were obtained using a high-resolution video camera and the related software, both of which were provided by the vendor.

2.6. Quantum chemical calculations

All molecular structures of suggested inhibitors were fully optimized by using PM3 semi-empirical method (46) as implemented in the program package HyperChem 7.52 with default gradient methods. No frozen core approximation was used throughout the calculations. All calculations were carried out in gas phase at 25°C.

3. Results and discussion

3.1. Chemical composition

3.1.1. FT-IR spectroscopy

The FT-IR results reveal that the peony leaves extract contains O, N, and P in the functional groups of alcohol, amine, aromatic ring, alkene, carbonyl, and phosphine oxide along with some alkane and alkyl halide. This is consistent with the typical chemistry of green inhibitors featuring organic compounds that contain heteroatoms which can adsorb onto the metallic surface and form a protective layer (23-27).

The FT-IR spectrum of the peony leaves extract is presented in Figure 1. A strong broad peak in the frequency of 3200-3500 cm⁻¹ together with a pair of medium peaks at 3427 and 3329 cm⁻¹ indicate the O-H stretch of alcohols and N-H stretch of amines. The small peak at 2914 cm⁻¹ could be attributed to the C-H stretch of alkane groups or =C-H stretch of alkenes. The peak at 1674 cm⁻¹ indicates the presence of C=O stretch (carbonyls) or -C=C- stretch (alkenes).

The adsorption band observed at 1595 cm⁻¹ was due to C-C stretch (in-ring) of aromatic compounds, whereas the peak at 1456 cm⁻¹ was attributed to C-H bend of alkanes or C-C stretch (in-ring) of aromatics. The peaks at 1149 and 1032 cm⁻¹ were due to P=O bond of phosphine oxides and C-N stretch of aliphatic amines, respectively. In addition, a band at 1362–1394 cm⁻¹

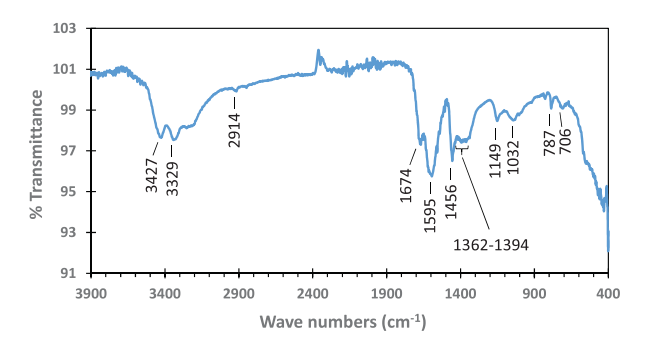


Figure 1. FT-IR spectrum of the peony leaves extract.

could be assigned to the C-H rock of alkane compounds. This is a special feature within the wagging band region of phospholipids (47, 48). Finally, the peaks at 787 and 706 cm⁻¹ were related to C-Cl stretch of alkyl halides, the source of which could be attributed to the protein used in the bacterial culture media (49).

3.1.2. Liquid chromatography-mass spectroscopy (LC-MS)

Liquid chromatography-mass spectrometry (LC-MS) results for the peony leaves extract are presented in Figure 2 and Table 3. According to the LC-MS results, peony leaves extract contains O, N, and P. As mentioned earlier, the organic compounds that contain these elements have a polar function. Therefore, they can be adsorbed on the surface of metal and form a protective layer.

3.2. Electrochemical characterization

3.2.1. LPR results

The temporal evolution of corrosion rate of the carbon steel in various inhibitor/NaCl solutions is shown in Figure 3. The corrosion current density was calculated following the Stern-Geary equation (50).

$$i_{\rm corr} = \frac{\beta_{\rm a}\beta_{\rm c}}{2.3(\beta_{\rm a} + \beta_{\rm c})} \frac{1}{R_{\rm p}},\tag{2}$$

where β_a and β_c are anodic and cathodic Tafel slopes, respectively, both assumed to be 100 mV/decade, a typical value for β . Polarization resistance (R_p , Ω) is equal to the slope of the polarization curve $(\Delta E/\Delta i)$ obtained using the LPR method. In this method, the sample is polarized, on the order of ±20 mV, relative to the OCP. The corrosion current density was then used directly to calculate the corrosion rate (in mpy or milli-

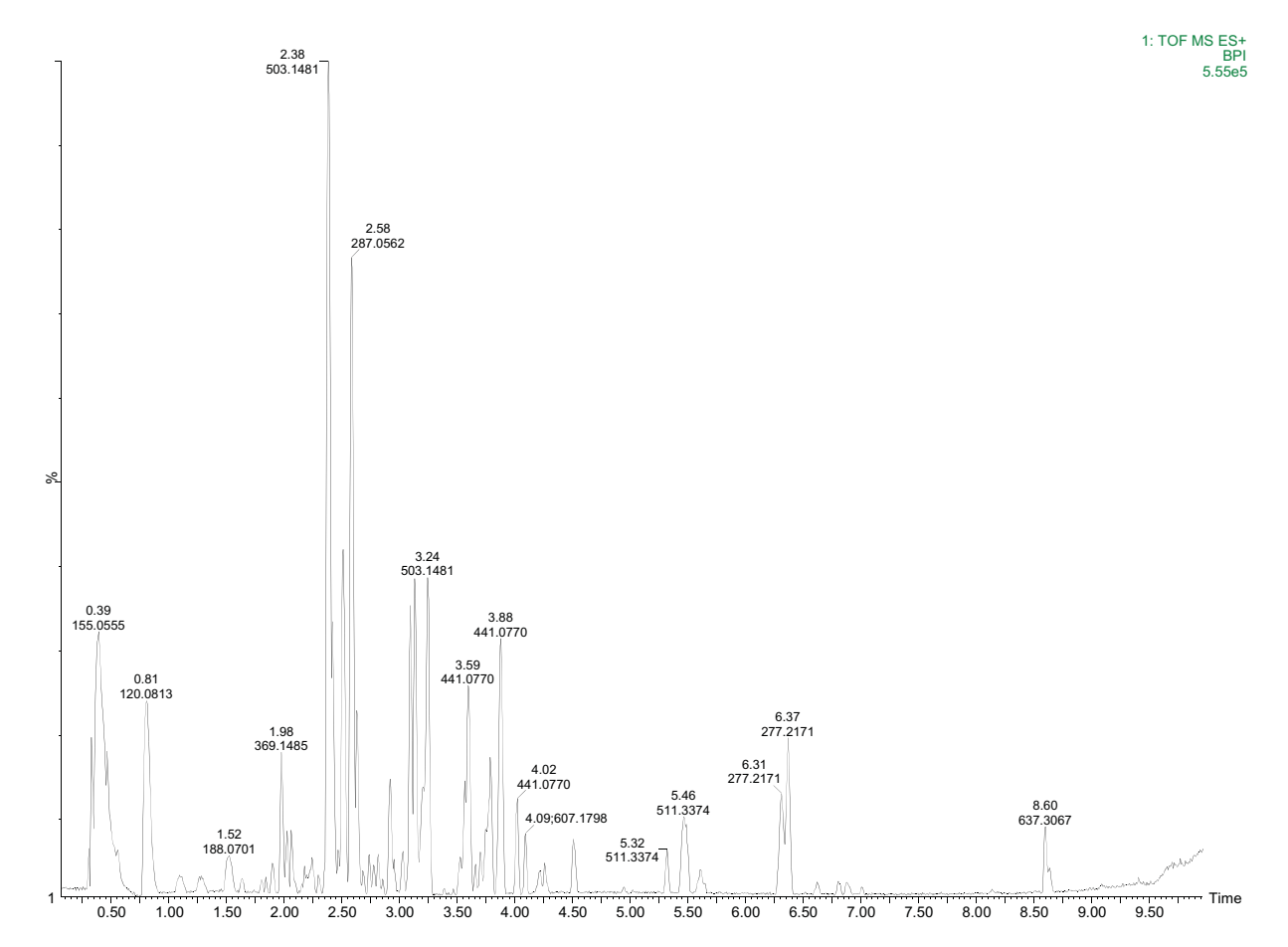


Figure 2. LC-MS chromatogram of peony leaves extract.



Table 3. Summary of the chemical constituents detected for peony leaves extract using LC-MS technique.

Formula	Retention time (min)	m/z		
C ₄ H ₁₀ O ₆	0.39	155.0555		
$C_{21}H_{22}N_6O_9$	2.38	503.1481		
$C_{15}H_{10}O_6$	2.58	287.0562		
C ₁₉ H ₂₇ N ₄ O ₁₀ P	3.24	503.1481		
$C_{16}H_{11}F_7N_4O_3$	3.59	441.0770		
$C_{17}H_{16}N_3O_9P$	3.88	441.0770		
$C_{16}H_{11}F_7N_4O_3$	4.02	441.0770		
$C_{29}H_{22}N_{10}O_6$	4.09	607.1798		
C ₂₇ H ₄₆ N ₂ O ₇	5.46	511.3374		
C ₁₈ H ₂₈ O ₂	6.37	277.2171		
C ₂₉ H ₄₈ O ₁₅	8.60	637.3067		

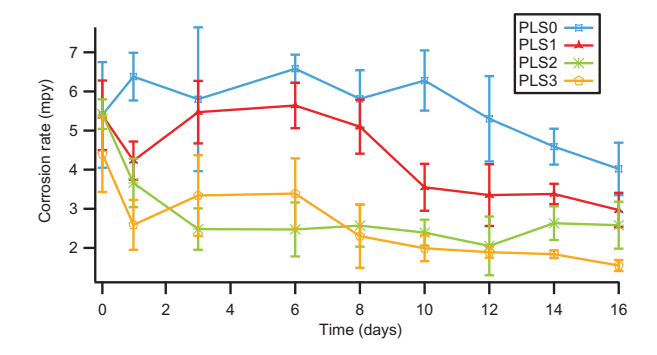


Figure 3. Corrosion rate (from LPR) versus time for C1010 steel in NaCl solutions containing 0–3 vol.% PLS.

inch per year), following the equation derived from the Faraday's law (51).

Corrosion rate (mpy) =
$$\frac{0.13 \times i_{corr} \times E.W.}{\rho}$$
, (3)

where E.W. is the equivalent weight of carbon steel (27.92 g), i_{corr} is the corrosion current density (in μ A cm⁻²) and ρ is the density of steel (7.87 g cm⁻³).

Figure 3 clearly illustrates that the presence of peony leaves extract solution (PLS) decreased the corrosion rate and therefore exhibited an inhibitory effect. This effect was particularly significant for the NaCl solutions with PLS at 2 or 3 vol.%. The inhibition effect was still outstanding even after 16 days of steel immersion. Such sustained inhibition is highly desirable, making this green inhibitor a promising candidate for formulating longlasting inhibitor packages.

3.2.2. PDP results

The PDP curves of the C1010 carbon steel coupons after 16 days of immersion in various inhibitor/NaCl solutions are shown in Figure 4. The steel coupons in the control group (PLSO, no inhibitor) exhibited the highest cathodic current density. There was no limiting diffusion current density observed in the cathodic curve and the anodic curve suggests that the steel was in the status of active dissolution. Note that the proposed anodic reactions

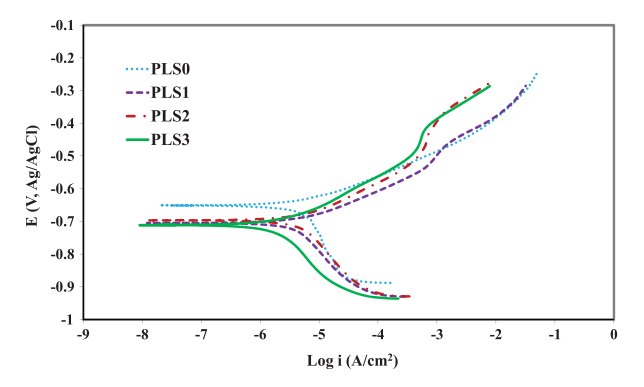


Figure 4. PDP curves for C1010 steel after 16-day immersion in NaCl solution containing 0–3 vol.% PLS.

for steel corrosion induced by chloride in near-neutral pH solutions are as follows (52).

$$Fe^{2+} + 2CI^{-} \rightarrow FeCl_{2}, \tag{4}$$

$$FeCl_2 + 2H_2O \rightarrow Fe(OH)_2 + 2H^+ + 2CI^-,$$
 (5)

$$6FeCl_2 + O_2 + 6H_2O \rightarrow 2Fe_3O_4 + 12H^+ + 12CI^-$$
. (6)

The main cathodic reaction in the presence of sufficient dissolved oxygen is as follows (53).

$$O_2 + 2H_2O + 4e^- \rightarrow 4OH^-.$$
 (7)

Figure 4 illustrates the beneficial effect of PLS on the corrosion behavior of the carbon steel in 3.5 wt.% NaCl. The addition of PLS at 1 vol.% shifted the cathodic current density to the passive direction and the corrosion potential (E_{corr}) to a more negative value. This is likely due to the adsorption of organic molecules on the cathodic active sites of steel surface (54, 55). By increasing the PLS concentration to 2 vol.%, the cathodic and anodic current densities further decreased, with more pronounced shift seen on the cathodic side. These trends continued when the PLS concentration was further increased to 3 vol.%. In the NaCl solutions containing PLS at various concentrations, the anodic branch of the polarization curve featured a current plateau, which is ascribed to desorption of strongly adsorbed inhibitor from the metallic surface (56, 57).

The electrochemical parameters obtained from the PDP curves are presented in Table 4. Corrosion current density (i_{corr}) decreased as the PLS concentration was increased up to 3 vol.%, where the lowest i_{corr} was obtained. The addition of PLS changed the anodic Tafel slope (β_a) slightly, but it changed the cathodic Tafel slope (β_c) considerably. This shows that PLS inhibits corrosion by mostly blocking the cathodic active sites (58). In fact, PLS is oxidized and acts as the anodic compared to steel (37). The increase in the cathodic Tafel slope also indicates that the addition of PLS changes the mechanism of the reduction reaction (59). The corrosion



Table 4. Electrochemical parameters fitted from polarization plots.

	Tafel slopes (mV/decade)				
Sample name	$oldsymbol{eta_{a}}$	βς	$E_{\rm corr}$ (mV)	$i_{\rm corr}$ (μ A/cm ²)	IE%*
PLS0	68.0 ± 10.0	401.3 ± 72.6	-635.1 ± 22.5	7.2 ± 0.7	_
PLS1	79.3 ± 0.1	298.1 ± 4.8	-706.5 ± 2.4	5.7 ± 0.3	20.2
PLS2	103.7 ± 8.3	218.9 ± 75.8	-704.8 ± 28.0	4.0 ± 2.5	43.9
PLS3	97.4 ± 4.2	241.5 ± 5.1	-708.3 ± 3.8	2.5 ± 0.3	65.3

^{*}IE% = $(1 - i_{corr (uninhibited)}/i_{corr (inhibited)}) \times 100$.

potential (E_{corr}) shifted to more negative potentials with the PLS concentration. Since the amount of this shift was less than 85 mV, this inhibitor is considered as a mixed type inhibitor with a predominating cathodic character (60).

In general, adsorption of a corrosion inhibitor on the surface of metal affects the corrosion process by decreasing the available area for corrosion reactions (geometric blocking effect) and/or by modifying the activation energy of the electrochemical reactions happening in the corrosion process (52). It is difficult to conclude which aspects of the inhibition mechanism are attributed to the geometric blocking effect and which ones are related to the energy effect. When there is a negligible change in the corrosion potential after addition of inhibitor, the geometric blocking effect is the main mechanism of inhibition. Since there is a considerable change in the corrosion potential values upon addition of PLS (Table 4), therefore the energy effect is the main inhibition mechanism, although the geometric blocking effect cannot be ignored.

3.2.3. EIS results

The impedance Nyquist plots of C1010 carbon steel in uninhibited and inhibited 3.5% NaCl solutions with different concentrations of PLS are shown in Figure 5. It is clear that the protection response of carbon steel was modified by the presence of different concentrations of the PLS and the increase in time. The real part of the surface impedance increases with the inhibitor concentration and time, reaching a maximum value with 3 vol.% of PLS inhibitor at day 16. This indicates that by increasing the concentration of PLS and over time, the density of the protective layer formed on the surface of metal is increased (61). Similar shape of the capacitive loops suggests that the corrosion inhibition process followed the same mechanism and is controlled by charge transfer process, regardless of the inhibitor concentration and immersion time. These loops are not perfect semi-circles and such deviation is attributed to frequency dispersion by the roughness or non-homogeneity of the working electrode surface caused by corrosion attack (28). Adsorption of the protective organic layer on the metal surface can also cause induce

surface heterogeneity and modify its impedance characteristics (62, 63).

The impedance modulus diagrams, Figure 6, show the rising trend of low frequency impedance value $|Z|_{5mHz}$ with increasing the concentrations of PLS and time. Therefore, it can be inferred that there is an increase in protection with increasing the concentrations of PLS and over immersion time (64). This might indicate that peony leaves extract exhibits an active protection. These results are in good agreement with LPR and Tafel polarization results.

The impedance Bode phase plots (Figure 6) show that the more time-of-exposure and PLS concentration results in the higher maximum phase angles, which reflects a capacitive behavior due to the increase of polarization resistance with increasing the concentrations of PLS and time. The control sample (PLS0) after 12 days of immersion and all of the samples exposed to the solutions with PLS showed two time constants at different frequency ranges which can be attributed to the change in surface morphology (65). This change may be related to the formation of a layer on the surface of steel. According to Cao (55), when the geometric blocking effect is the main mechanism of corrosion inhibition by the adsorbed inhibitive species on the metallic surface, one time constant is distinguished in the EIS plots. If the inhibition is not controlled by the geometric blocking effect, the EIS plot will possess two time constants. Therefore, according to the EIS results it can be concluded that the inhibition is not controlled by the geometric blocking effect. This is in good agreement with the PDP results and confirms that the inhibition is mainly caused by the energy effect.

Figure 7 presents the equivalent electrical circuit employed to investigate the impedance spectra at day 16 of the test. In this figure, R_s is the uncompensated solution resistance, R_f is the corrosion product film resistance which is the electrical resistance due to the formation of ionically conducting paths in the film, Q_f is the constant phase element (CPE) of the corrosion product film, R_{ct} is the charge transfer resistance indicative of the corrosion resistance of the metal, and $Q_{\rm dl}$ is the CPE of double layer at the metal/electrolyte interface. The CPEs represent non-ideal capacitors in the EIS data,

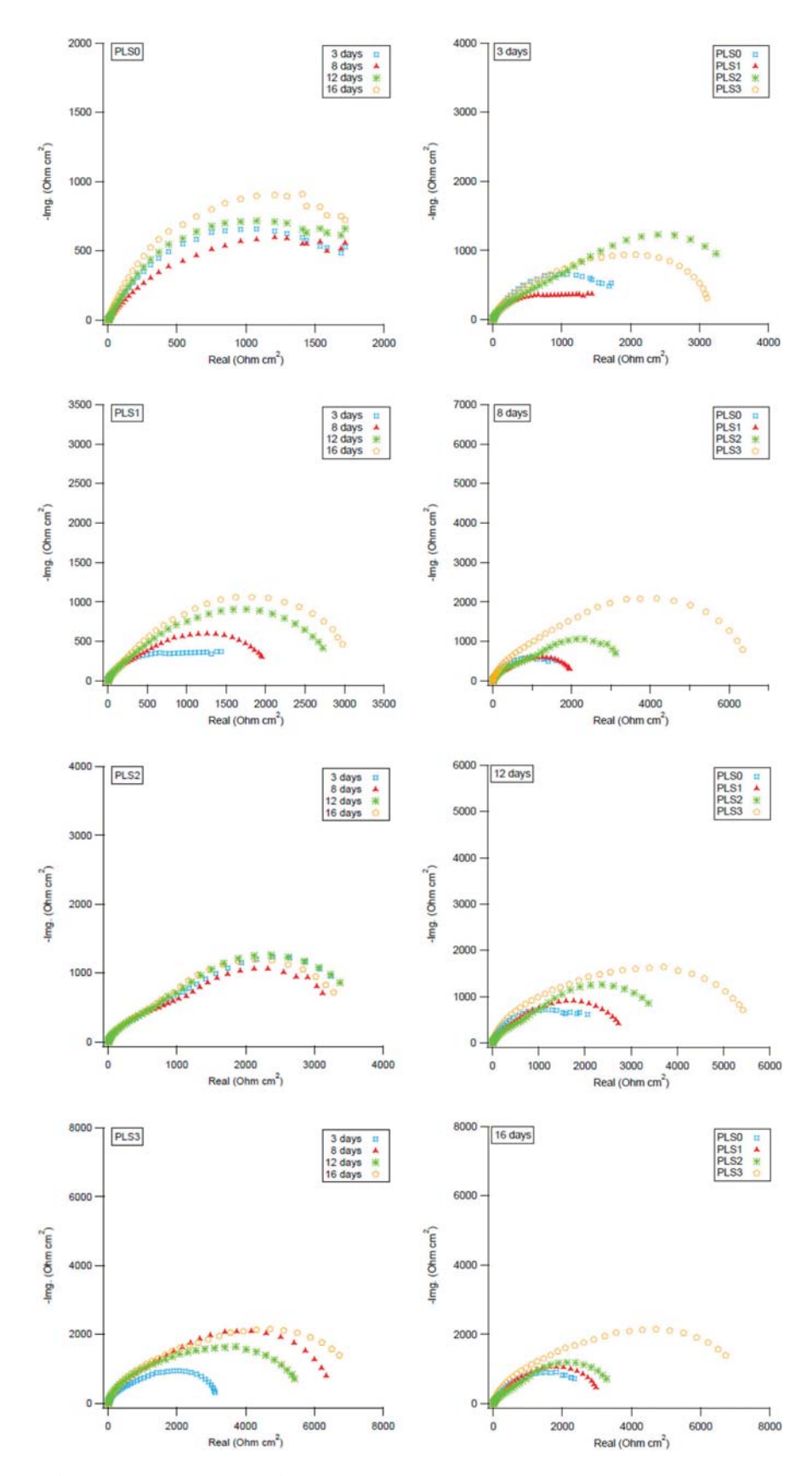


Figure 5. Nyquist plots for C1010 steel vs. time (left column) and vs. PLS concentration (right column) in NaCl solution containing 0–3 vol.% PLS.

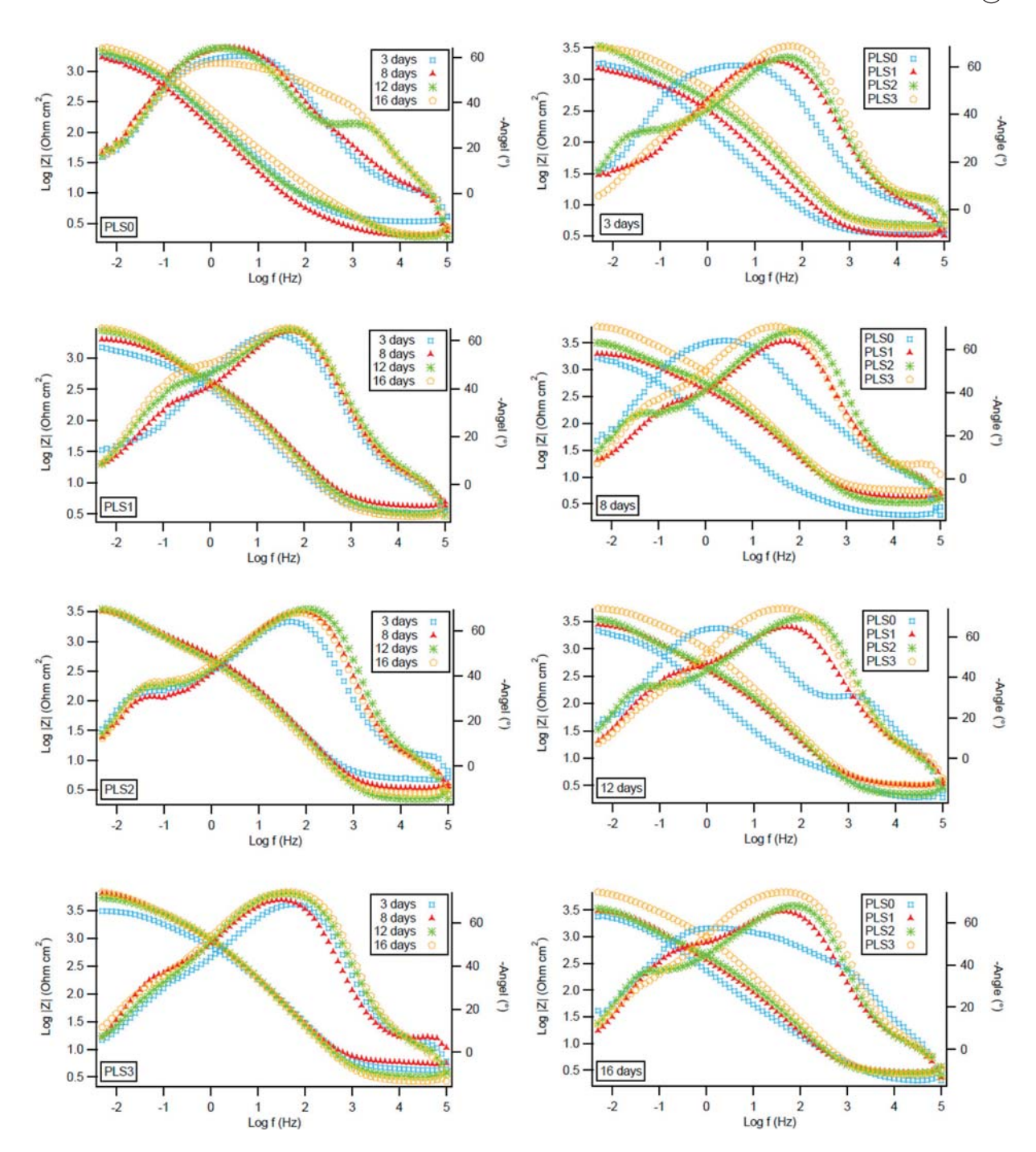


Figure 6. Impedance Bode modulus plots for C1010 steel vs. time (left column) and vs. PLS concentration (right column) in NaCl solution containing 0–3 vol.% PLS.

and their impedance is expressed as follows (66).

$$Z_{\text{CPE}} = \frac{1}{Y_0(jw)^n},\tag{8}$$

where Y_0 is the magnitude of the CPE, and $-1 \le n \le 1$. The higher frequency range loops have depressed semicircular appearance, $0.5 \le n \le 1$, which is often referred to the frequency dispersion as a result of the non-homogeneity or the roughness of the solid surface (67, 68).

The $C_{\rm dl}$ values were calculated as follows (69).

$$C_{\rm dl} = (Y_0 R_{\rm ct}^{1-n})^{1/n}.$$
 (9)

Figure 8 shows the Nyquist plot, the impedance modulus diagram, the impedance Bode phase plot and the fitted data for PLS3 sample. There is a good agreement between the experimental results and the fitted data.

Table 5 summarizes the values of the fitted parameters. The value of $C_{\rm dl}$ decreased with the increase

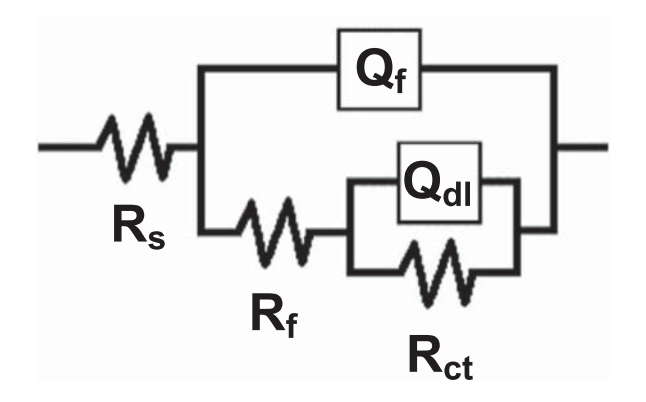


Figure 7. Equivalent circuit model used to analyse the EIS results.

in the concentration of PLS, revealing that the organic inhibitor molecules interfered the metal/electrolyte interface. The decrease in $C_{\rm cl}$ value can be attributed to the decrease of dielectric constant (ε) or the increase of thickness (δ) of the double layer, according to the following equation (40).

$$C_{\rm dl} = \frac{\varepsilon \varepsilon_0 A}{\delta},\tag{10}$$

where ε_0 is the vacuum permittivity and A, is the electrode surface area exposed to the electrolyte.

Table 5 also illustrates that $R_{\rm ct}$ value increased while $C_{\rm dl}$ value decreased with the increase in the concentration of PLS, suggesting that the inhibitor performance was due to the adsorption of inhibitor molecules on the metal surface (70). Usually, the higher $R_{\rm ct}$ values are associated with slower rate of corrosion process (71). As such, the $R_{\rm ct}$ values confirm that the PLS inhibition efficiency increased with its concentration (at day 16). The decrease of $C_{\rm dl}$ value can be attributed to the

decrease in the local dielectric constant and the increase in the thickness of electric double layer (61). This shows that the water molecules and other ions on the surface of metal have been displaced by peony leaves extract molecules through adsorption at the metal/solution interface (72).

The Nyquist plots of the C1010 steel samples in 3.5% NaCl solutions containing different concentrations of the SWPL are shown in Figure 9. It is obviously seen that increasing the concentration of SWPL does not have any significant effect on the corrosion behavior of the C1010 carbon steel samples. This shows that the protection obtained by PLS is due to the peony leaves.

3.3. Adsorption isotherm

The interaction between the organic compounds and metal surfaces can be explained from the basic information of adsorption isotherm. To clarify the adsorption type of peony leaves extract on C1010 carbon steel, the degree of surface coverage (θ) were assumed to be equivalent of inhibition efficiency (IE) obtained by PDP results. The experimental results of IE (at day 16) versus peony leaves extract concentration (C, in g/L, dry mass per volume of corresponding green solution) were fitted to a variety of different adsorption isotherms. Among them, the Frumkin isotherm showed the best correlation coefficient of 0.995 (Figure 10), which is governed by the following equation (73).

$$\log\left(\frac{\theta C}{1-\theta}\right) = 2\alpha\theta + 2.303\log K,\tag{11}$$

where K is the adsorption–desorption constant and α is the lateral interaction term. The calculated values for α

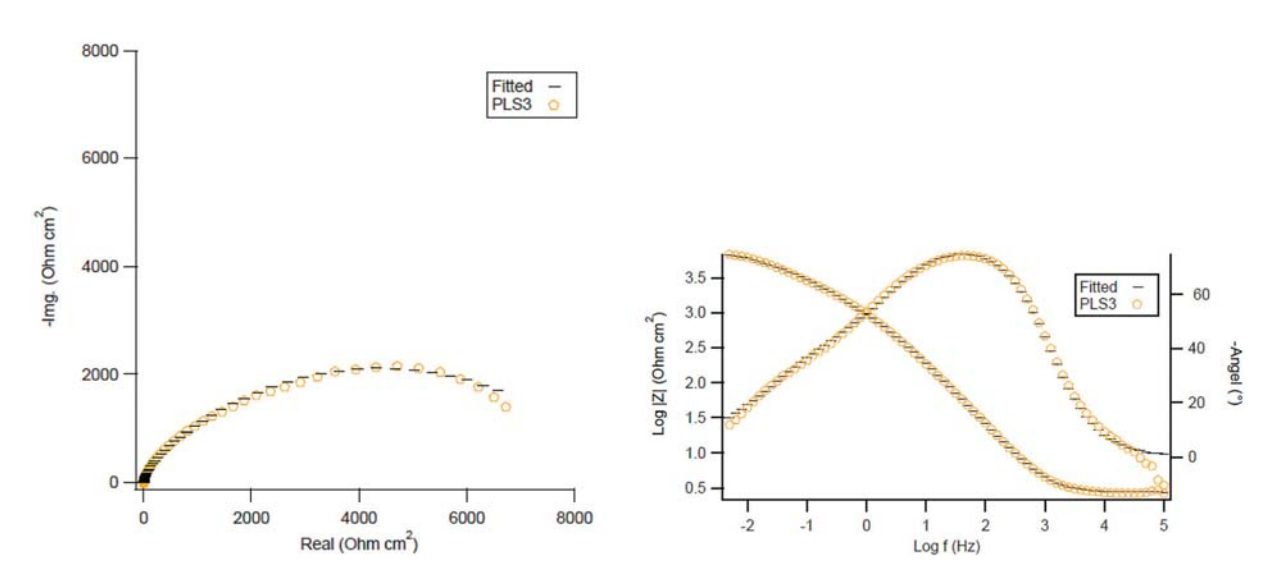


Figure 8. Nyquist plot (left column) and impedance Bode phase plot (right column) with the fitted curves for C1010 steel immersed in NaCl solution containing 3 vol.% PLS after 16 days.



Table 5. Electrochemical impedance parameters obtained by fitting EIS data to equivalent circuit in Figure 7.

			Q_{f}			Q_{dl}			
Sample name	$R_{\rm s}~(\Omega~{\rm cm}^2)$	$R_{\rm f}~(\Omega~{\rm cm}^2)$	$\gamma_{0f} (\Omega^{-1} \text{ cm}^{-2} \text{ s}^{nf}) \times 10^{-5}$	n_{f}	$R_{\rm ct}~(\Omega~{\rm cm}^2)$	$(\Omega^{-1} \text{ cm}^{-2} \text{ s}^{\text{ndl}}) \times 10^{-4}$	n _{dl}	$C_{\rm dl} \ ({\rm F \ cm^{-2}}) \times 10^{-4}$	IE%*
PLS0	2.2 ± 0.1	4.5 ± 1.7	6.1 ± 5.9	0.96 ± 0.04	2610.3 ± 464.3	13.7 ± 2.4	0.67 ± 0.01	25.6	_
PLS1	2.8 ± 0.4	388.3 ± 104.0	29.1 ± 0.8	0.85 ± 0.01	3739 ± 694.3	6.9 ± 1.6	0.62 ± 0.08	12.3	30.2
PLS2	2.9 ± 0.1	103.5 ± 151.5	9.3 ± 8.5	0.94 ± 0.06	4780.3 ± 626.1	4.4 ± 4.0	0.58 ± 0.11	7.6	45.4
PLS3	2.6 ± 0.3	454.9 ± 628.5	8.2 ± 5.6	0.95 ± 0.07	7627.5 ± 675.3	2.5 ± 1.4	0.61 ± 0.11	3.8	65.8

^{*}IE% = $(1 - R_{ct \text{ (uninhibited)}}/R_{ct \text{ (inhibited)}}) \times 100.$

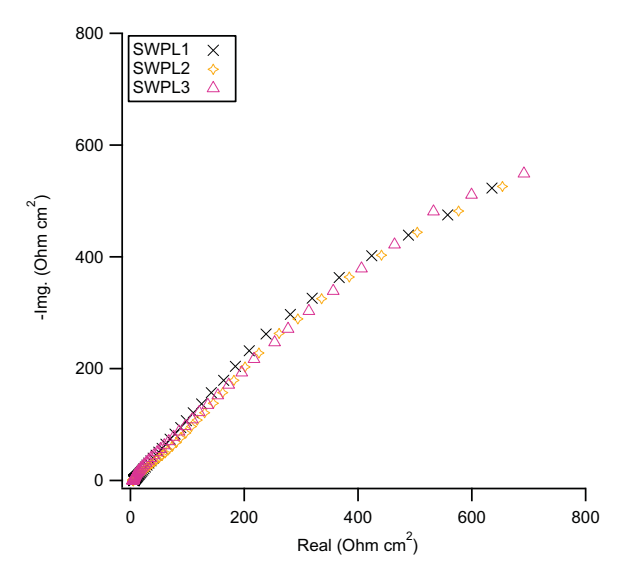


Figure 9. Nyquist plots for C1010 steel after 16-day immersion in NaCl solution containing 1–3 vol.% of solution without peony leaves (SWPL1-3).

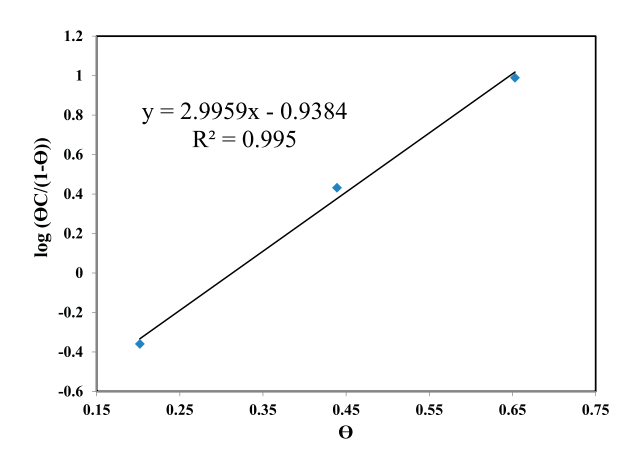


Figure 10. Adsorption isotherm for the peony leaves extract on C1010 carbon steel after 16-day immersion in NaCl solution containing 0–3 vol.% PLS.

and log*K* are 1.4980 and -0.4075, respectively. The Frumkin isotherm is an extension of the Langmuir isotherm in describing certain adsorption phenomena. Classical isotherms of adsorption (Frumkin, Langmuir, Henry) are based on the model of non-penetrable interface,

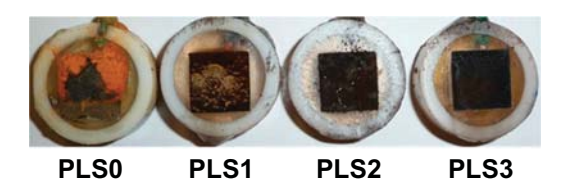


Figure 11. Digital photo of steel coupons after 16-day immersion in NaCl solution containing 0–3 vol.% PLS.

where an adsorbate can substitute only molecules of one solvent. The Frumkin model is the main model that accounts for non-ideal interactions of both insoluble-soluble (1–2) and/or soluble-soluble (2–2) components (74).

Subsequently, the Gibbs free energy of adsorption (ΔG_{ads}^0) was calculated as follows (73, 75).

$$\Delta G_{\text{ads}}^0 = -2.303 \text{RTlog}(C_{\text{solvent}}K),$$
 (12)

where R is the gas constant (8.314 J K⁻¹ mol⁻¹), T is the absolute temperature (room temperature 298 K), $C_{\rm solvent}$ is the concentration of water which is approximately 1000 g/L, and K is the adsorption constant (L/g). By substituting the value of logK in Equation 12, $\Delta G_{\rm ads}^0$ was estimated to be -14.79 kJ mol⁻¹. The negative value of Gibbs free energy indicates that the adsorption process occurred spontaneously. Since the absolute value of $\Delta G_{\rm ads}^0$ is less than 20 kJ mol⁻¹, this suggests physical adsorption in which electrostatic interaction occurs between inhibitor molecules and metal surface (26).

3.4. Surface analyses

3.4.1. Digital photo

The surface morphology of steel coupons after 16-day continuous exposure to various inhibitor/NaCl solutions is depicted in Figure 11. The surface layer in the 3.5 wt.% NaCl with higher inhibitor concentrations (e.g. PLS at 3 vol.%) was more uniform and complete. The steel coupon exposed to uninhibited salt brine (PLS0) was partially covered by orange rust. The brown color of the layer formed on the PLS1 coupon shows that this layer was partially composed of rust. The color of the adsorbed layers on the surface of PLS2 and PLS3

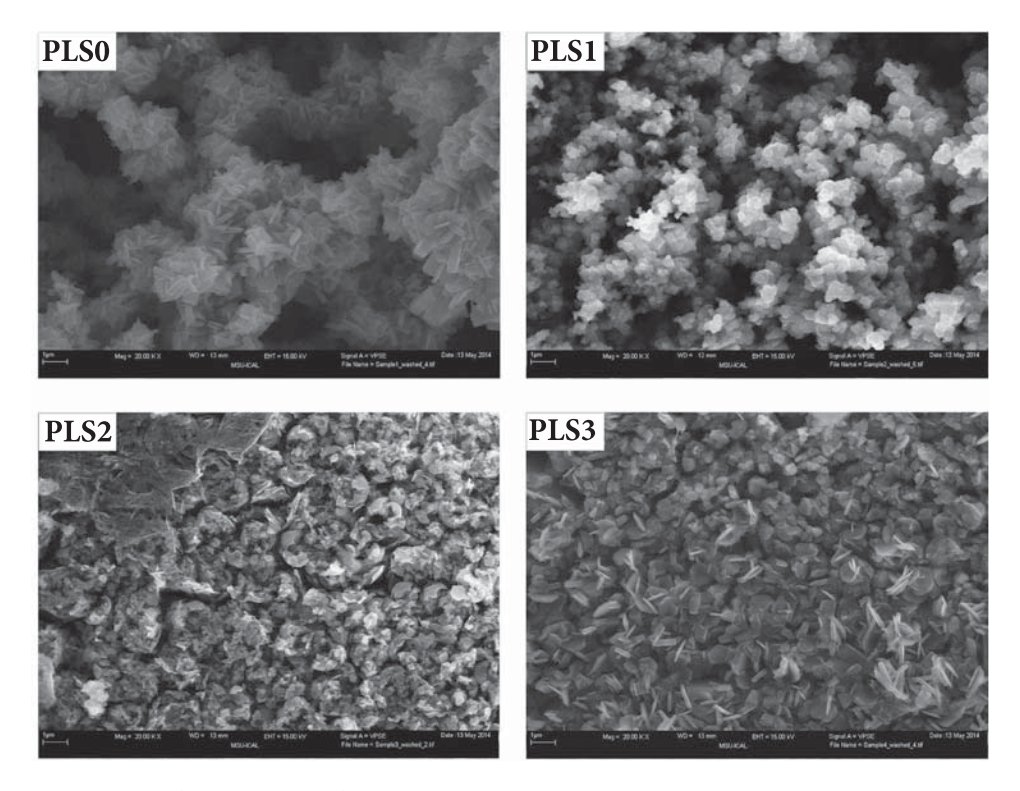


Figure 12. FESEM micrographs of steel coupons after 16-day immersion in NaCl solution containing 0 to 3 vol.% PLS. The length of scale bar is 1 µm in all samples.

coupons was black, implying that the chemical composition of the surface layers on these samples differed from that on the PLSO coupon.

3.4.2. FESEM micrographs of rust layer

The microstructural level morphology of steel rust layer after 16-day continuous exposure to various inhibitor/ NaCl solutions was further examined by FESEM, as shown in Figure 12. The micrographs confirm that more porous rust layers formed on the steel surfaces exposed to salt brine with no inhibitor (PLS0) or low inhibitor concentration (PLS1). In contrast, a relatively dense layer with submicron pores formed on the steel surface in the presence of higher inhibitor concentrations (PLS2 and PLS3). It is known that more compact corrosion product layer is attributed to less corrosion rate (76, 77). Therefore, these data are in good agreement with electrochemical measurements, which revealed lower corrosion rates of PLS2 and PLS3 steel coupons.

3.4.3. XRD results

The crystalline phases in the surface layer of the aforementioned steel coupons were examined by XRD, as shown in Figure 13. On the steel surface exposed to uninhibited 3.5 wt.% NaCl (PLSO), the peaks associated with NaCl, Fe, γ-FeOOH, and Fe₃O₄ can be observed. The

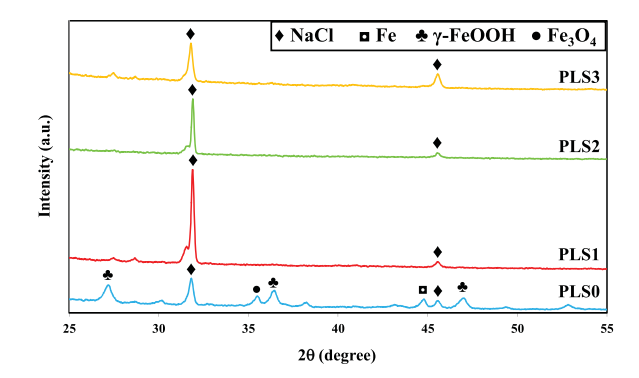


Figure 13. XRD patterns of the corrosion product layer on C1010 carbon steel in NaCl solution containing 0 to 3 vol.% PLS.

number and intensity of the peaks associated with y-FeOOH were more than those of Fe₃O₄, suggesting that γ-FeOOH was the dominant iron oxide/hydroxide phase (78, 79). For the steel surface exposed to inhibited 3.5 wt.% NaCl (PLS1, PLS2, and PLS3), only NaCl was detected, implying that either the surface consisted of mainly NaCl crystals or the thickness of the surface layer is less than the resolution of XRD method.

3.4.4. XPS results

For more in-depth analysis of the corrosion surface layer on PLS3 steel coupon, XPS analysis was employed, which enables simultaneous detection of different elements.

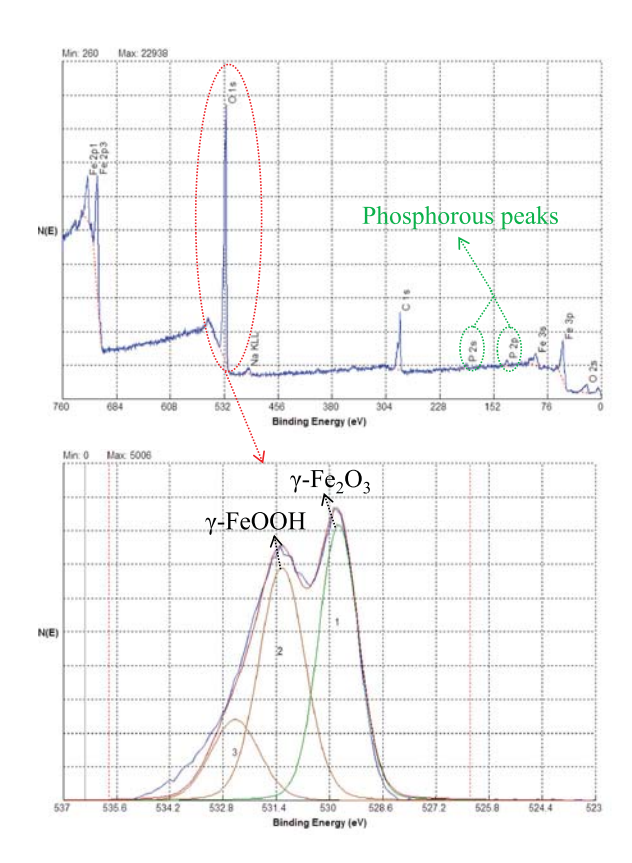


Figure 14. XPS results for PLS3 steel coupon.

The presence of P in the corrosion product layer is obviously detected. This, along with the LC-MS results, reveal that $C_{19}H_{27}N_4O_{10}P$ and $C_{17}H_{16}N_3O_9P$ are the main active ingredients in the PLS. Phosphate-based compounds have a higher negative charge density than amine based ones (80) which were observed in LC-MS and FT-IR results; as such, phosphate-based compounds can form stronger and more stable bonds with the metallic surface. The XPS results reveal that the iron oxide phase in the corrosion surface layer is made of two phases, y-Fe₂O₃ and y-FeOOH, as shown in Figure 14. From the combination of XRD and XPS results, it can be concluded that in the presence of peony leaves extract, all of the Fe₃O₄ phase and some of the γ-FeOOH were converted to γ-Fe₂O₃. Fe₂O₃ can adhere to the surface of steel as a passive layer and provide a barrier against further corrosion attack by chlorides. This shows that the organic molecules acted as the catalyst (81). It is known that phosphate-based compounds can act as catalyst at neutral pH and cause oxygen evolution reaction (82). In this study, C₁₉H₂₇N₄₋ O₁₀P and C₁₇H₁₆N₃O₉P acted as catalysts in converting Fe₃O₄ and γ -FeOOH to γ -Fe₂O_{3.}

3.4.5. SEM micrographs of as-washed samples

The SEM micrographs of the surface of carbon steel samples after removing the rust layer are shown in

Figure 15. Uniform corrosion was observed on the control sample (PLSO, uninhibited) and on the samples immersed in the 3.5 wt.% NaCl solutions containing higher inhibitor concentrations (PLS2 and PLS3). Pitting corrosion was recognized on the sample tested in the 3.5 wt.% NaCl containing 1 vol.% of peony leaves extract solution (PLS1), suggesting inadequate protection by the inhibitor despite the reduction in average corrosion rate (indicated by the electrochemical measurements). This finding is consistent with the surface coverage by adsorbed organic layer presented in Figure 11.

3.5. Contact angle and surface free energy

Water contact angle was measured to determine the degree of surface hydrophilicity of the carbon steel samples in the presence or absence of the PLS. Then the surface free energy (y_{sv}) was calculated using the following formula (83, 84).

$$W_A = \gamma_{lv}(1 + \cos\theta), \tag{13}$$

$$W_{\rm A} = 2(\gamma_{\rm lv}\gamma_{\rm sv})^{1/2} \exp[-\beta(\gamma_{\rm lv}-\gamma_{\rm sv})^2],$$
 (14)

where W_A is the work of adhesion, γ_{lv} is the surface tension of water which is 71.97 mJ/m² at 25°C, θ is water contact angle, and β is a constant equal to $0.0001247 \text{ (mJ/m}^2)^{-2}$.

The addition of the peony leaves extract liquid to 3.5 wt.% NaCl increased the contact angle and decreased the surface free energy, as depicted in Figure 16. These changes can be attributed to an adsorbed hydrophobic layer on the surface of carbon steel (83, 85), further validating the findings from electrochemical and surface analyses. In summary, the adsorption mechanism of peony leaves derivatives displaced water molecules from the carbon steel surface. The decrease in the surface free energy indicates the aggregation of inhibitor molecules on the surface of carbon steel and formation of a protective adsorbed layer (86).

3.6. Quantum chemical calculations

Quantum chemical calculations were run on C₁₉H₂₇N₄₋ O₁₀P and C₁₇H₁₆N₃O₉P molecules which were determined as the main active ingredients in the PLS. Their molecular modeling was calculated after the geometries were fully relaxed. The stable geometries of the molecules were obtained using the PM3 method that implemented in Hyperchem package, as shown in Figure 17. Non-flat conformations of C₁₉H₂₇N₄O₁₀P and C₁₇H₁₆N₃O₉P were the most stable geometries for these compounds due to the minimum angle and

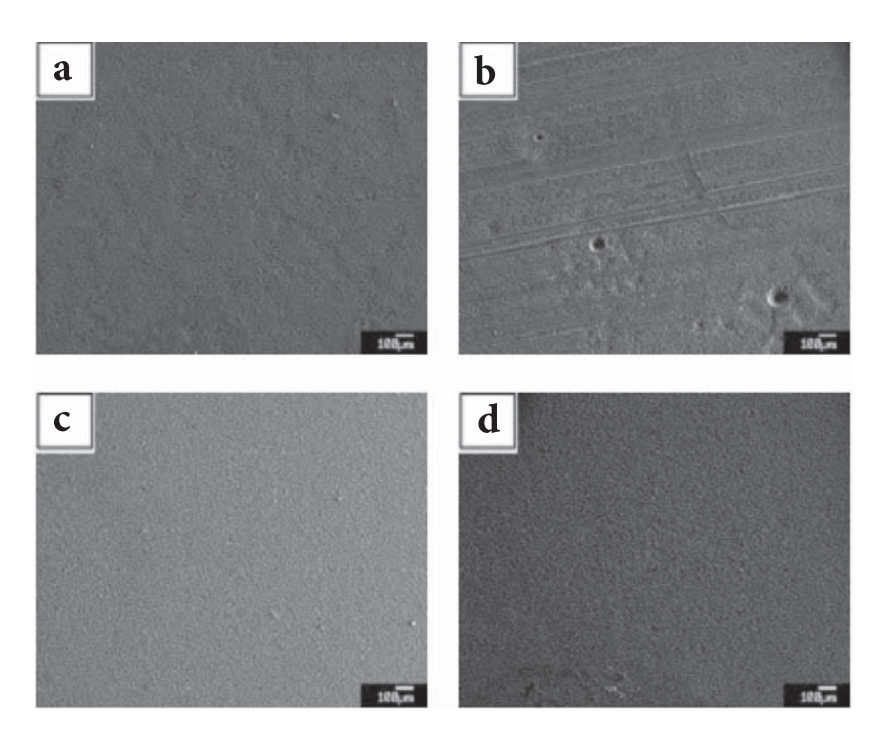


Figure 15. SEM micrographs of as-washed steel surface after 16-day immersion in 3.5% NaCl solution with PLS at (a) 0 vol.%, (b) 1 vol.%, (c) 2 vol.%, and (d) 3 vol.%. The scale in all images represents 100 μm.

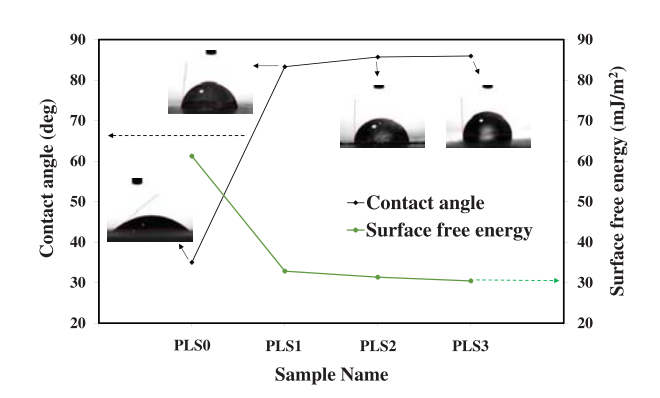


Figure 16. Measured water contact angle and surface energy for different samples.

torsional strains. Although non-planar conformations of $C_{19}H_{27}N_4O_{10}P$ and $C_{17}H_{16}N_3O_9P$ was used, the intra Hbonding could not be achieved between the hydrogen atom of N or the oxygen atom with closed atoms of N or O. For C₁₉H₂₇N₄O₁₀P, the calculations showed Hbonding between NH₃ moiety and HO-group of amidophosphate moiety.

The calculations for C₁₉H₂₇N₄O₁₀P predicted that the formal charges on nitrogen, oxygen, and phosphorus atoms were (-0.558 to +0.047), (-0.682 to -0.36) and (+2.090) e/atom, respectively. The formal charges on carbon atoms were found to be (-0.265 to +0.298) e/atom. The average formal charge from the hydrogen

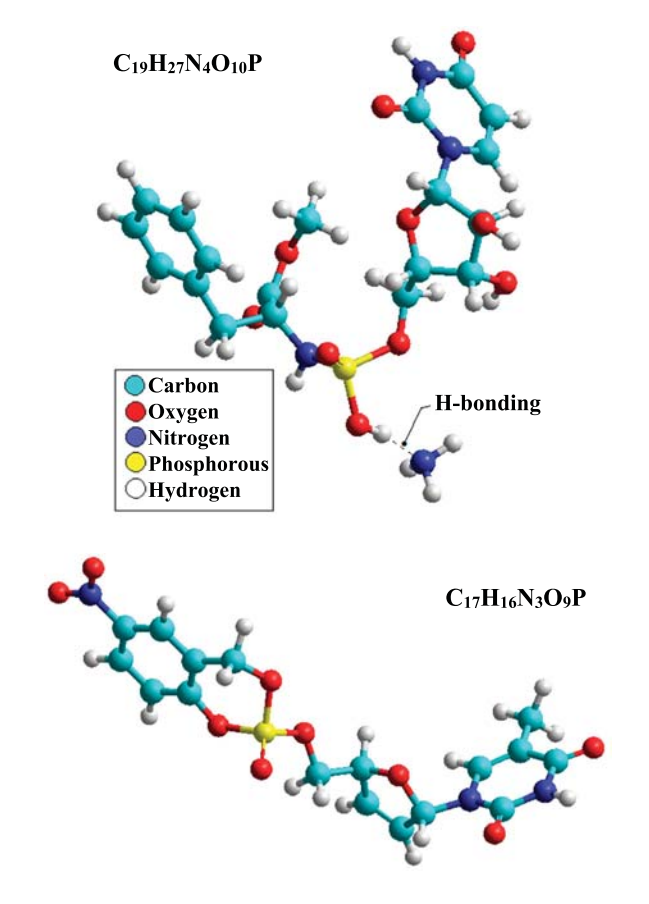


Figure 17. Conformation structure for C₁₉H₂₇N₄O₁₀P and C₁₇H₁₆-N₃O₉P molecules obtained using PM3 method.

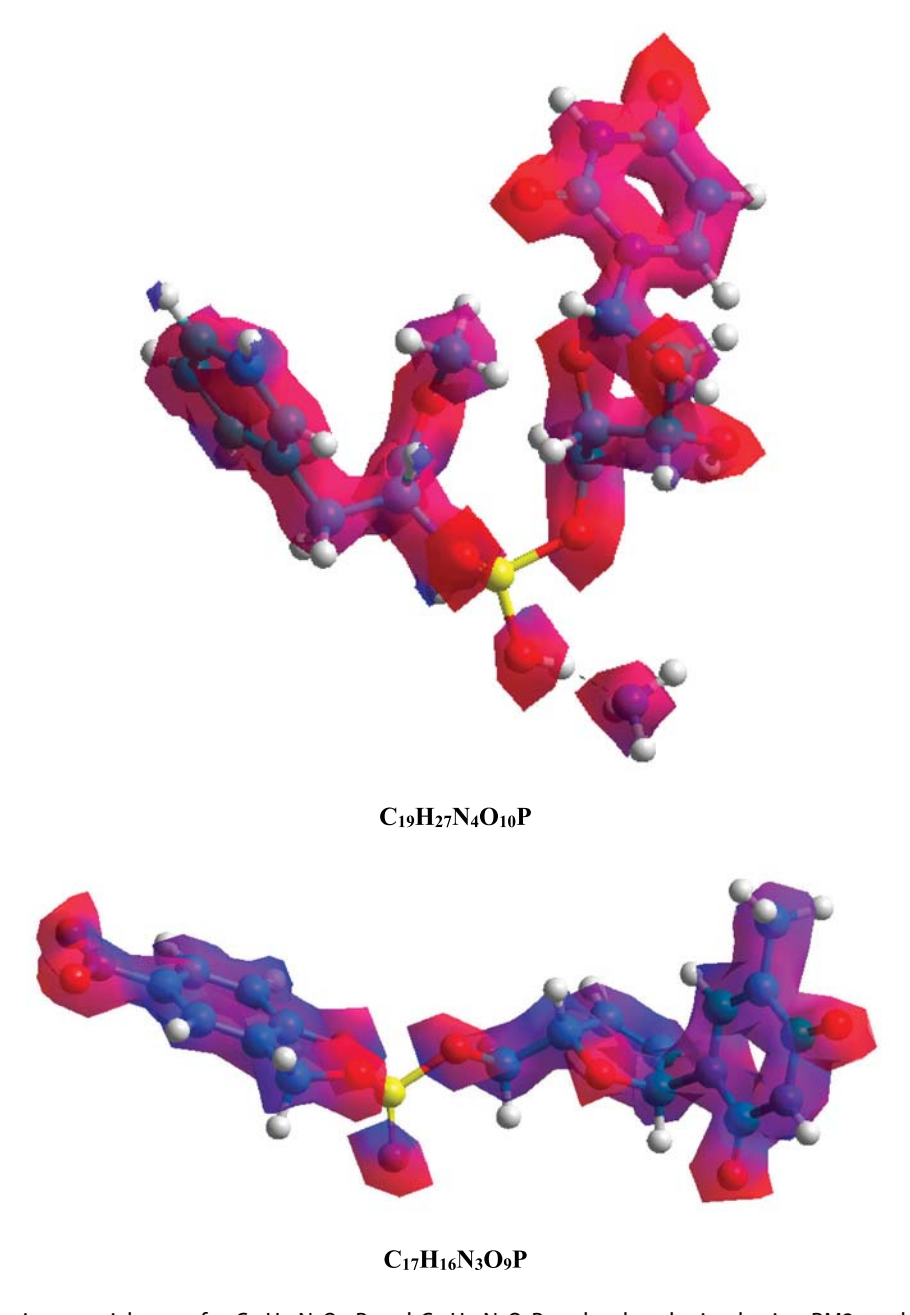
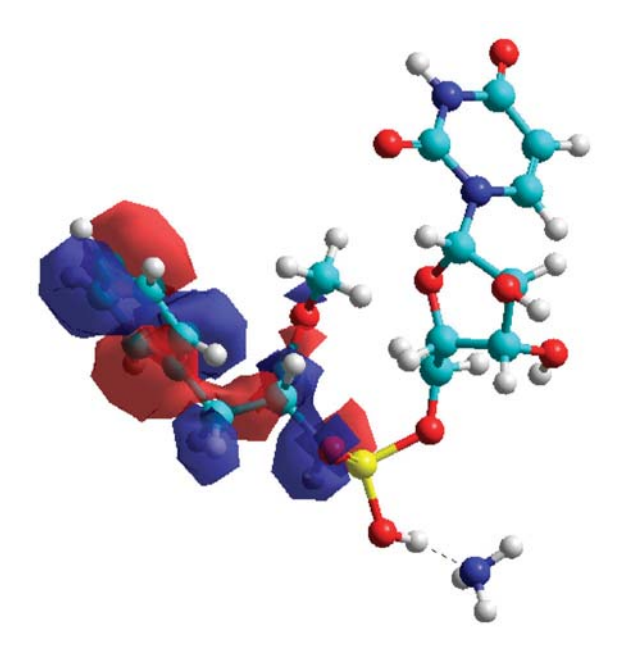


Figure 18. Electrostatic potential maps for C₁₉H₂₇N₄O₁₀P and C₁₇H₁₆N₃O₉P molecules obtained using PM3 method.

atoms was about (+0.110) e/atom. The difference in the electronic density distribution on full molecular modeling system of C₁₉H₂₇N₄O₁₀P leads to a dipole moment (μ) value of 8.07 D (Debye) for this compound. The calculations for C₁₇H₁₆N₃O₉P predicted that the formal charges on nitrogen, oxygen and phosphorus atoms were (+1.318 to -0.018), (-0.352 to -0.833), and (+2.187) e/atom, respectively. The formal charges on carbon atoms were found to be (+0.305 to -0.469) e/atom. The average formal charge from the hydrogen atoms was about (+1.135) e/atom. The difference in the electronic density distribution on full molecular modeling gives a μ value of 5.44 D for $C_{17}H_{16}N_3O_9P$. Higher

values of the dipole moment will improve corrosion inhibition efficiency (87). The calculations show that $C_{19}H_{27}$ N₄O₁₀P and C₁₇H₁₆N₃O₉P molecules have high dipole moment values, which exhibits their good corrosion inhibitory efficacy.

Figure 18 shows the electrostatic potential energy maps of the molecular modeling systems of C₁₉H₂₇N₄₋ O₁₀P and C₁₇H₁₆N₃O₉P. It illustrates the charge distributions of three-dimensional molecules. These maps assist in visualization of the variable charged regions of these molecules. There is a difference in the distribution of electronic density and energy levels which gives $E_{\text{LUMO}} = -0.4155 \text{ eV}$ $E_{\text{HOMO}} = -9.5630 \text{ eV}$ and



номо

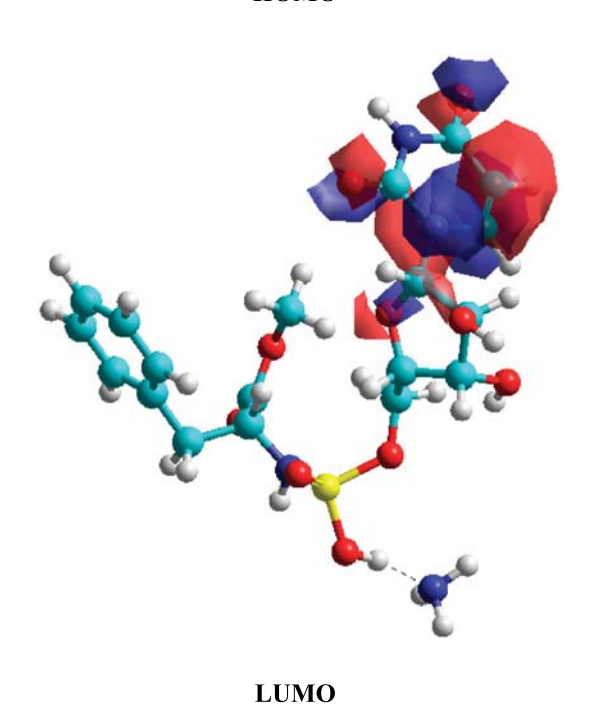


Figure 19. The isosurfaces of frontier molecular orbital density distributions for C₁₉H₂₇N₄O₁₀P molecule obtained using PM3 method.

 $C_{19}H_{27}N_4O_{10}P$ and $E_{HOMO} = -9.5077 \text{ eV}$ and $E_{LUMO} =$ -1.0518 eV for $C_{17}H_{16}N_3O_9P$. Such differences could lead to the interaction with other reactive sites.

Figures 19 and 20 show the frontier molecular orbitals (HOMO and LUMO) respectively for C₁₉H₂₇N₄O₁₀P and C₁₇H₁₆N₃O₉P. The calculated HOMO-LUMO gap energies $(\Delta E = E_{LUMO} - E_{HOMO})$ were 9.1475 and 8.4559 eV for C₁₉- $H_{27}N_4O_{10}P$ and $C_{17}H_{16}N_3O_9P$, respectively. The energy gap has high value in both molecules due to the absence of contribution of conjugated system of aromatic ring. The isosurfaces of the orbital HOMO are localized in the molecule of $C_{19}H_{27}N_4O_{10}P$ through amidophosphate moiety, whereas the side chain (ester group and benzene ring) made with a slightly contribution to the electronic distribution of the HOMO in molecular modeling. The amidophosphate moiety and ester group with benzene ring are the reactive site (donor) of molecular modeling system C₁₉H₂₇N₄O₁₀P to achieve adsorption processes on the metal surface by N and O atoms. The isosurfaces of the orbital HOMO are localized in the molecule C₁₇H₁₆N₃O₉P through the pyrimidine ring. Pyrimidine ring is the reactive site (donor) of molecular modeling system C₁₇H₁₆N₃O₉P to achieve adsorption processes on the metal surface by N and O atoms. In contrast, LUMO as an acceptor, where the electronic distribution is localized in the N, O, and P atoms of pyrimidine moiety and nitrobenzene moiety in the molecular modeling systems of $C_{19}H_{27}N_4O_{10}P$ and $C_{17}H_{16}N_3O_9P$, respectively. The acceptor moiety has an important role to coordinate with negatively ions in the environments.

This theoretical study showed that the methyl and aromatic groups attached to the molecular modeling system of C₁₉H₂₇N₄O₁₀P, and alkyl and olefin groups attached to the molecular modeling system of C₁₇H₁₆N₃₋ O₉P had no effect on either the HOMO or the LUMO distributions, but they could work as hydrophobic fragments. Calculation of quantum chemical parameters for $C_{19}H_{27}N_4O_{10}P$ and $C_{17}H_{16}N_3O_9P$ indicates that these compounds are efficient corrosion inhibitors, which corresponds to the experimental results.

Finally, we suggest that $C_{19}H_{27}N_4O_{10}P$ and $C_{17}H_{16}N_{3-}$ O₉P have inhibition effects due to the interaction of the lone pair of electrons on the heteroatoms (N, O) and those on the heteroatoms of the pyrimidine ring with the metal surface, respectively. These interactions form a kind of valuable co-ordination with the metal surface through the spontaneous adsorption processes. Figure 21 shows suggested physisorption mechanism for the molecules of C₁₉H₂₇N₄O₁₀P and C₁₇H₁₆N₃O₉P on the surface of metal.

3.7. Mechanism of corrosion inhibition

The mechanism of inhibition was formation of a protective layer due to the adsorption of peony leaves extract molecules onto the steel surface. The adsorption mechanism followed the Frumkin adsorption isotherm through the physical adsorption in which electrostatic interaction occurs between inhibitor molecules and metal surface. The Frumkin model is the main model that accounts for non-ideal interactions of both

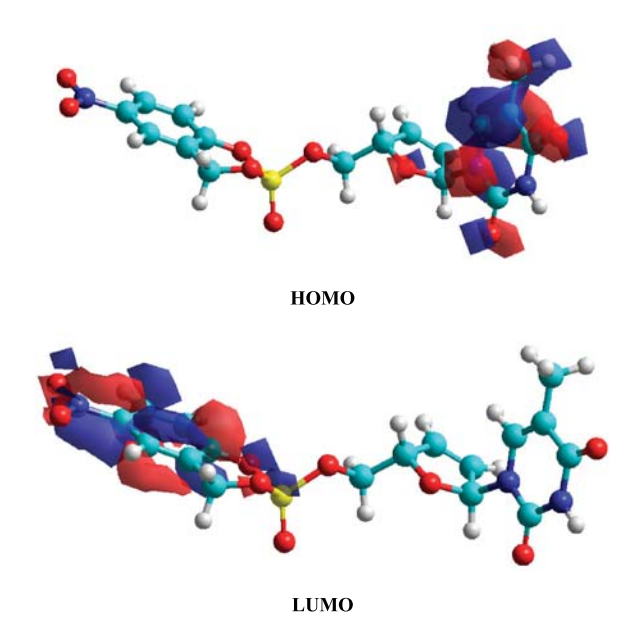


Figure 20. The isosurfaces of frontier molecular orbital density distributions for C₁₇H₁₆N₃O₉P molecule obtained using PM3 method.

insoluble-soluble and/or soluble-soluble components. The corrosion inhibition was mainly due to the adsorption of $C_{19}H_{27}N_4O_{10}P$ and $C_{17}H_{16}N_3O_9P$ molecules, as active ingredients, which also induce the formation of y-Fe₂O₃ as a passive layer on the steel. The adsorption of these molecules was attributed to the interaction of the lone pair of electrons on the heteroatoms (N, O) with the metal surface.

The adsorption process caused an increase in the hydrophobicity of the surface and a decrease in the surface free energy. Higher PLS concentration resulted in a larger charge transfer resistance (R_{ct}) and a lower double-layer capacitance ($C_{\rm dl}$). The former is related to the corrosion inhibition and the latter is attributed to the decrease in the local dielectric constant and increase in the thickness of electric double layer. This showed that the water molecules and other ions on the surface of steel have been displaced by PLS molecules through the adsorption at the steel/solution interface.

The corrosion inhibition increases with the concentration of the PLS and over immersion time, which shows that this inhibitor exhibits an active protection. It inhibits corrosion by blocking the cathodic active sites and is oxidized compared to steel. Addition of PLS changes the mechanism of the reduction reaction and shifts the corrosion potential to more negative values. The amount of this shift is less than 85 mV, therefore, this inhibitor is considered as a mixed type inhibitor with a predominating cathodic character.

4. Conclusions

This work describes the corrosion inhibition behavior of a novel liquid "green inhibitor" derived from peony leaves using a novel chemical and biological degradation process. The corrosion inhibition of C1010 carbon steel in 3.5% NaCl was studied by electrochemical measurements and surface analyses and the key findings are summarized as follows.

(1) The inhibition efficiency increased with increasing the concentration of peony leaves extract, from 0% to 3 vol.%. Used at 3 vol.%, this green inhibitor exhibited a good inhibition efficiency of 65.8% after 16 days of steel immersion time, based on PDP test.

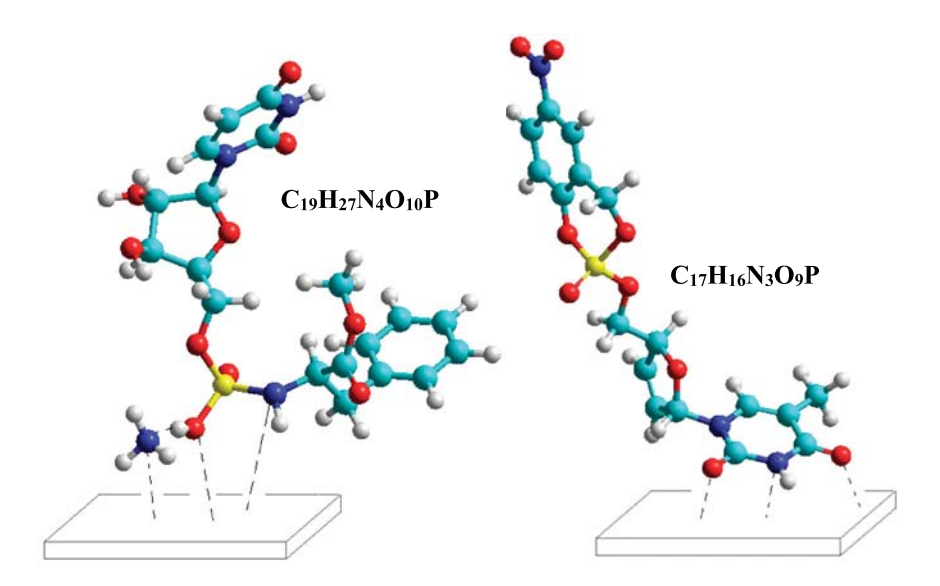


Figure 21. Suggested physisorption mechanism for C₁₉H₂₇N₄O₁₀P and C₁₇H₁₆N₃O₉P molecules.

- (2) The adsorption of PLS molecules follows the Frumkin adsorption isotherm through the physical adsorption in which electrostatic interaction occurs between inhibitor molecules and metal surface.
- (3) The peony leaves extract is a mixed type inhibitor with a predominating cathodic character that blocks the cathodic active sites on the surface of carbon steel, while acting as a catalyst in converting Fe_3O_4 and γ -FeOOH to γ -Fe₂O₃.
- (4) Addition of the extract increases the hydrophobicity of the steel surface and decreases the surface free energy.
- (5) The corrosion inhibition by peony leaves extract was mainly due to the adsorption of C₁₉H₂₇N₄O₁₀P and C₁₇H₁₆N₃O₉P molecules, as active ingredients which induce the formation of y-Fe2O3 as a passive layer on the steel.
- (6) A good correlation was found between experimentally determined inhibition efficiency and theoretically calculated properties of PLS using semiempirical calculations with PM3 method.
- (7) It is highly recommended to study the synergistic effect of a cation and PLS on the corrosion inhibition properties in the future researches.
- (8) Further studies are highly recommended to optimize the novel chemical/biological process of extracting green inhibitors introduced in this research.

Acknowledgements

The contents of this work reflect the views of the authors, who are responsible for the facts and the accuracy of the data presented herein. The mentioning of trademarks is for reader's convenience only and does not imply any endorsement.

Disclosure statement

No potential conflict of interest was reported by the authors.

Funding

The authors gratefully acknowledge financial support by the U.S. DOT Center for Environmentally Sustainable Transportation in Cold Climates (CESTiCC) and the National Natural Science Foundation of China (Project 51278390). The authors acknowledge the funding by NSF CRISP Program (Award 1638384).

Notes on contributors

Mehdi Honarvar Nazari completed Ph.D. in Metallurgical & Materials Engineering in 2010 at the University of Tehran, Iran and worked as a Postdoctoral Research Associate and Laboratory Manager at the Western Transportation Institute, USA and Washington State University (WSU). He is currently pursuing his 2nd Ph.D. in Environmental Engineering at WSU, and his research ranges from bio-based deicers, anti-corrosion coatings, to microbial fuel cells.

Mehdi Salih Shihab received his B.Sc. degree from Baghdad University (1986) in Chemistry and his M.Sc. in Organic Chemistry (1995) at same University. He received his Ph.D. in Physical Organic Chemistry at Kazan federal University-Russia (2002). He worked as a Research Associate at A. M. Butlerov Chemical Institute, Kazan State University for one year (2002-2003). The period of 2003- 2005 of his research life was spent as Postdoctoral Research Associate at Oita University, Japan. Since 2005, he has been a Professor in the Chemistry Department, Al-Nahrain University, Iraq.

Ling Cao received her B.S. in Oceanic Science from Hebei University, China (2005) and M.Sc. in Microbiology at Huazhong Agricultural University, China (2009). She worked as a Research Associate at the Department of Microbiology and Immunology, Montana State University, USA in 2010-2012, and then at the Western Transportation Institute, USA in 2012-2014.

Eden Adele Havens received her B.S. in Civil Engineering from the Voiland College of Engineering and Architecture at Washington State University in 2016 as well as a B.A. in Applied Physics from Whitworth University at the same time. She currently works as an engineer for the Northwest Region of Washington State Department of Transportation in the Traffic Safety and Design Office.

Xianming Shi is an Associate Professor in the Department of Civil and Environmental Engineering and the Site Director of Center for Environmentally Sustainable Transportation in Cold Climates at Washington State University. He holds a Ph.D. in Chemistry from Institute of Chemistry, Chinese Academy of Sciences (1999), a M.S. in Applied Chemistry from Tianjin University, China (1996), a B.S. in Corrosion & Protection from Beijing University of Chemical Technology, China (1993), and a 2nd M.S. in Industrial & Management Engineering from Montana State University, USA (2002). His research interests are focused on innovative materials and practices for sustainable transportation infrastructure.

ORCID

Xianming Shi http://orcid.org/0000-0003-3576-8952

References

- [1] Shi, X.; Veneziano, D.; Xie, N.; Gong, J. Use of Chloride-Based Ice Control Products for Sustainable Winter Maintenance: A Balanced Perspective. Cold Reg. Sci. Technol. **2013**, 86,104–112.
- [2] Usman, T.; Fu, L.; Miranda-Moreno, L.F. Quantifying Safety Benefit of Winter Road Maintenance: Accident Frequency Modeling. Accid. Anal. Prev. 2010, 42, No. 6, 1878–1887.
- [3] Ye, Z.; Veneziano, D.; Shi, X. Estimating Statewide Benefits of Winter Maintenance Operations. Transp. Res. Rec. J. Transp. Res. Board. 2013, 2329,17-23.
- [4] Anning, D.W.; Flynn, M.E. Dissolved-Solids Sources, Loads, Yields, and Concentrations in Streams of the Conterminous United States. U. S. Geological Survey Scientific Investigations, Scientific Investigations Report Report 2014-5012, 2014.



- [5] Corsi, S.R.; Graczyk, D.J.; Geis, S.W.; Booth, N.L.; Richards, K.D. A Fresh Look at Road Salt: Aquatic Toxicity and Water-Quality Impacts on Local, Regional, and National Scales. Environ. Sci. Technol. 2010, 44, No. 19, 7376-7382.
- [6] Kelly, V.R.; Findlay, S.E.G.; Schlesinger, W.H.; Menking, K.; Chatrchyan, A.M. Road Salt: Moving Toward the Solution. The Cary Institute of Ecosystem Studies, Special Report, 2010.
- [7] Nazari, M.H.; Fay, L.; Jungwirth, S.; Shi, X. Water Quality Implications and the Toxicological Effects of Chloride-Based Deicers. In Environmental Sustainability in Transportation Infrastructure, American Society of Civil Engineers: Fairbanks, 2015; pp 272-292.
- [8] Thunqvist, E.-L. Regional Increase of Mean Chloride Concentration in Water Due to the Application of Deicing Salt. Sci. Total Environ. 2004, 325, Nos. 1–3, 29–37.
- [9] Lundmark, A.; Olofsson, B. Chloride Deposition and Distribution in Soils along a Deiced Highway -Assessment Using Different Methods of Measurement. Water. Air. Soil Pollut. 2007, 182, Nos. 1-4, 173-185.
- [10] Gałuszka, A.; Migaszewski, Z.M.; Podlaski, R.; Dołęgowska, S.; Michalik, A. The Influence of Chloride Deicers on Mineral Nutrition and the Health Status of Roadside Trees in the City of Kielce, Poland. Environ. Monit. Assess. 2011, 176, Nos. 1-4, 451-464.
- [11] Fay, L.; Shi, X. Environmental Impacts of Chemicals for Snow and Ice Control: State of the Knowledge. Water Air Soil Pollut., 2012, 223,2751-2770.
- [12] Li, Y.; Fang, Y.; Seeley, N.; Jungwirth, S.; Jackson, E.; Shi, X. Corrosion by Chloride Deicers on Highway Maintenance Equipment: Renewed Perspective and Laboratory Investigation. Transp. Res. Rec. J. Transp. Res. Board. **2013,** *2361,*106–113.
- [13] Siegel, L. Hazard Identification for Human and Ecological Effects of Sodium Chloride Road Salt. New Hampshire Department of Environmental Services, Final Report, July 2007.
- [14] Teien, H.-C.; Garmo, Ø.A.; Åtland, Å.; Salbu, B. Transformation of Iron Species in Mixing Zones and Accumulation on Fish Gills. Environ. Sci. Technol. 2008, 42, No. 5, 1780-1786.
- [15] Vuori, K.-M. Direct and Indirect Effects of Iron on River Ecosystems. Ann. Zool. Fennici., 1995, 32, 317-329.
- [16] Wang, H.; Yao, H.; Sun, P.; Pei, J.; Li, D.; Huang, C.-H. Oxidation of Tetracycline Antibiotics Induced by Fe(III) lons Without Light Irradiation. Chemosphere. 2015, 119, 1255-1261.
- [17] Vardy, D.W.; Santore, R.; Ryan, A.; Giesy, J.P.; Hecker, M. Acute Toxicity of Copper, Lead, Cadmium, and Zinc to Early Life Stages of White Sturgeon (Acipenser transmontanus) in Laboratory and Columbia River Water. Environ. Sci. Pollut. Res. 2014, 21, No. 13, 8176-8187.
- [18] Li, Y.; Zhang, Y.; Jungwirth, S.; Seely, N.; Fang, Y.; Shi, X. Corrosion Inhibitors for Metals in Maintenance Equipment: Introduction and Recent Developments. Corros. Rev. 2014, 32, No. 5-6, 163-181.
- [19] Muthumani, A.; Shi, X. Effectiveness of Liquid Agricultural By-Products and Solid Complex Chlorides for Snow and Ice Control. J. Cold Reg. Eng. 2017, 31, No. 1, p. 04016006.
- [20] de Souza, F. S.; Spinelli, A. Caffeic Acid as a Green Corrosion Inhibitor for Mild Steel. Corros. Sci. 2009, 51, No. 3, 642-649.

- [21] Obot, I.B.; Gasem, Z.M.; Umoren, S.A. Molecular Level Understanding of the Mechanism of Aloes Leaves Extract Inhibition of Low Carbon Steel Corrosion: A DFT Approach. Int. J. Electrochem. Sci. 2014, 9, 510-522.
- [22] Patni, N.; Agarwal, S.; Shah, P.; Patni, N.; Agarwal, S.; Shah, P. Greener Approach Towards Corrosion Inhibition, Greener Approach Towards Corrosion Inhibition. Chin. J. Eng. Chin. J. Eng. 2013, 2013, e784186.
- [23] Eddy, N.O.; Ekwumemgbo, P.A.; Mamza, P.A.P. Ethanol Extract of Terminalia catappa as a Green Inhibitor for the Corrosion of Mild Steel in H2SO4. Green Chem. Lett. Rev. **2009,** 2, No. 4, 223–231.
- [24] Kamal, C.; Sethuraman, M.G. Spirulina Platensis A Novel Green Inhibitor for Acid Corrosion of Mild Steel. Arab. J. Chem., 2012, 5, No. 2, 155-161.
- [25] Senthilkumar, A.N.; Tharini, K.; Sethuraman, M.G. Corrosion Inhibitory Effect of Few Piperidin-4-One Oximes on Mild Steel in Hydrochloric Acid Medium. Surf. Rev. Lett. 2009, 16, No. 01, 141-147.
- [26] Solmaz, R. Investigation of Corrosion Inhibition Mechanism and Stability of Vitamin B1 on Mild Steel in 0.5 M HCl Solution. Corros. Sci., 2014, 81, 75-84.
- [27] Trabanelli, G. Corrosion Inhibitors. In Corrosion Mechanisms, 1st ed.Marcel Dekker Inc.: New York, 1987; pp 119-164.
- [28] Al-Amiery, A.A.; Binti Kassim, F.A.; Kadhum, A.A.H.; Mohamad, A.B. Sci. Rep. 2016, 6. DOI:10.1038/srep19890
- [29] Benabdellah, M.; Touzani, R.; Aouniti, A.; Dafali, A.; El Kadiri, S.; Hammouti, B.; Benkaddour, M. Inhibitive Action of Some Bipyrazolic Compounds on the Corrosion of Steel in 1 M HCl: Part I: Electrochemical Study. Mater. Chem. Phys. 2007, 105, Nos. 2-3, 373-379.
- [30] Shihab, M.S.; Honarvar Nazari, M.; Fay, L. Study of Inhibition Effect of Pyridinium Salt Derivative on Corrosion of C1010 Carbon Steel in Saline Solution. Prot. Met. Phys. Chem. Surf. 2016, 52, No. 4, 714-720.
- [31] Soltani, N.; Behpour, M.; Ghoreishi, S.M.; Naeimi, H. Corrosion Inhibition of Mild Steel in Hydrochloric Acid Solution by Some Double Schiff Bases. Corros. Sci. 2010, 52, No. 4, 1351-1361.
- [32] Yetri, Y.; Emriadi ;Jamarun, N.; Gunawarman. Corrosion Inhibition of Environmental Friendly Inhibitor Using Theobroma cacao Peels Extract on Mild Steel in NaCl Solution. J. Chem. Pharm. Res. 2015, 7, No. 5, 1083–1094.
- [33] Chen, S.; Singh, A.; Wang, Y.; Liu, W.; Deng, K.; Lin, Y. Inhibition Effect of Ilex Kudingcha C.J. Tseng (Kudingcha) Extract on J55 Steel in 3.5wt% NaCl Solution Saturated with CO2. Int. J. Electrochem. Sci. 2017, 12, 782-796.
- [34] Challouf, H.; Souissi, N.; Ben Messaouda, M.; Abidi, R.; Madani, A. Origanum majorana Extracts as Mild Steel Corrosion Green Inhibitors in Aqueous Chloride Medium. J. Environ. Prot. 2016, 7, 532-544.
- [35] Kusumastuti, R.; Pramana, R.I.; Soedarsono, J.W.; Fatimah, I.; Purwiandono, G. The Use of Morinda citrifolia as a Green Corrosion Inhibitor for Low Carbon Steel in 3.5% NaCl Solution. AIP Conf. Proc. 2017, 1823, No. 1, p. 020012.
- [36] Tuaweri, T.J.; Ogbonnaya, E.A.; Onyemaobi, O.O. Corrosion Inhibition of Heat Treated Mild Steel with Neem Leave Extract in a Chloride Medium. Int. J. Res. Eng. Technol., **2015,** 4, No. 6, 404-409.



- [37] Pradityana, A.; Sulistijono, A.; Shahab, A.; Noerochim, L.; Susanti, D. Inhibition of Corrosion of Carbon Steel in 3.5% NaCl Solution by Myrmecodia pendans Extract. Int. J. Corros. 2016, 2016, 1-6.
- [38] Nordrum, A. Flowers from Alaska. The Atlantic, 18-Jun-2014.
- [39] Cai, J.; Zhang, L. Rapid Dissolution of Cellulose in LiOH/ Urea and NaOH/Urea Aqueous Solutions. Macromol. Biosci. 2005, 5, No. 6, 539-548.
- [40] Behpour, M.; Ghoreishi, S.M.; Khayatkashani, M.; Soltani, N. Green Approach to Corrosion Inhibition of Mild Steel in Two Acidic Solutions by the Extract of Punica granatum Peel and Main Constituents. Mater. Chem. Phys., 2012, 131, No. 3, 621-633.
- [41] Chauhan, L.R.; Gunasekaran, G. Corrosion Inhibition of Mild Steel by Plant Extract in Dilute HCl Medium. Corros. Sci. 2007, 49, No. 3, 1143-1161.
- [42] Bammou, L.; Chebli, B.; Salghi, R.; Bazzi, L.; Hammouti, B.; Mihit, M.; Idrissi, H. Thermodynamic Properties of Thymus satureioides Essential Oils as Corrosion Inhibitor of Tinplate in 0.5 M HCl: Chemical Characterization and Electrochemical Study. Green Chem. Lett. Rev. 2010, 3, No. 3, 173-178.
- [43] Muthukrishnan, P.; Jeyaprabha, B.; Prakash, P. Mild Steel Corrosion Inhibition by Aqueous Extract Hyptissuaveolens Leaves. Int. J. Ind. Chem. 2014, 5, No. 1, 1–11.
- [44] Rodriguez-Clemente, E.; Gonzalez-Rodriguez, Valladares-Cisneros, M.G.; Chacon-Nava, J.G. Evaluation of Allium sativum as Corrosion Inhibitor for Carbon Steel in Sulphuric Acid under Hydrodynamic Conditions. Green Chem. Lett. Rev. 2015, 8, No. 2, 49-58.
- [45] Bouroushian, M.; Kosanovic, T. Characterization of Thin Films by Low Incidence X-ray Diffraction. Cryst. Struct. Theory Appl. 2012, 01, No. 03, 35.
- [46] Stewart, J.J.P. Optimization of Parameters Semiempirical Methods I. Method. J. Comput. Chem. **1989,** 10, 2, 209-220.
- [47] Lewis, R.N.; McElhaney, R.N.; Monck, M.A.; Cullis, P.R. Studies of Highly Asymmetric Mixed-Chain Diacyl Phosphatidylcholines that Form Mixed-Interdigitated Gel Phases: Fourier Transform Infrared and 2H NMR Studies of Hydrocarbon Spectroscopic Conformation and Orientational Order in the Liquid-Crystalline State. Biophys. J. 1994, 67, No. 1, 197-207.
- [48] Wolfangel, P.; Lehnert, R.; Meyer, H.H.; Müller, K. FTIR Studies of Phospholipid Membranes Containing Monoacetylenic Acyl Chains. Phys. Chem. Chem. Phys. 1999, 1, No. 20, 4833-4841.
- [49] Carugo, O. Buried Chloride Stereochemistry in the Protein Data Bank. BMC Struct. Biol. 2014, 14, 19.
- [50] Stern, M.; Geaby, A.L. Electrochemical Polarization I. A Theoretical Analysis of the Shape of Polarization Curves. J. Electrochem. Soc. 1957, 104, No. 1, 56-63.
- [51] Ezuber, H.M. Influence of Temperature and Thiosulfate on the Corrosion Behavior of Steel in Chloride Solutions Saturated in CO2. Mater. Des. 2009, 30, No. 9, 3420-3427.
- [52] Al Juhaiman, L.A.; Abu Mustafa, A.; Mekhamer, W.K. Polyvinyl Pyrrolidone as a Green Corrosion Inhibitor of Carbon Steel in Neutral Solutions Containing NaCl: Electrochemical and Thermodynamic Study. Int. J. Electrochem. Sci. 2012, 7, 8578-8596.

- [53] Sherif, E.-S.M.; Almajid, A.A. Electrochemical Corrosion Behavior of API X - 70 5L Grade Steel in 4.0 wt.% Sodium Chloride Solutions after Different Immersion Periods of Time. Int. J. Electrochem. Sci., 2015, 10, 34-45.
- [54] Abd El-Lateef, H.M.; Abu-Dief, A.M.; Abdel-Rahman, L.H.; Sañudo, E.C.; Aliaga-Alcalde, N. Electrochemical and Theoretical Quantum Approaches on the Inhibition of C1018 Carbon Steel Corrosion in Acidic Medium Containing Chloride Using Some Newly Synthesized Phenolic Schiff Bases Compounds. J. Electroanal. Chem. **2015,** 743, 120-133.
- [55] Cao, C. On Electrochemical Techniques for Interface Inhibitor Research. Corros. Sci. 1996, 38, No. 12, 2073-2082.
- [56] Feng, Y.; Siow, K.S.; Teo, W.K.; Hsieh, A.K. The Synergistic Effects of Propargyl Alcohol and Potassium Iodide on the Inhibition of Mild Steel in 0.5 M Sulfuric Acid Solution. Corros. Sci. 1999, 41, No. 5, 829-852.
- [57] Liu, X.; Okafor, P.C.; Zheng, Y.G. The Inhibition of CO2 Corrosion of N80 Mild Steel in Single Liquid Phase and Two-Phase Flow by Aminoethyl Liquid/Particle Imidazoline Derivatives. Corros. Sci. 2009, 51, No. 4, 744-751.
- [58] Soror, T.Y. Saffron Extracts as Environmentally Safe Corrosion Inhibitors for Aluminium Dissolution in 2M HCl Solution. Eur. Chem. Bull. 2013, 2, No. 4, 191-196.
- [59] Benabdellah, M.; Yahyi, A.; Dafali, A.; Aouniti, A.; Hammouti, B.; Ettouhami, A. Corrosion Inhibition of Steel in Molar HCl by Triphenyltin2–Thiophene Carboxylate. Arab. J. Chem. 2011, 4, No. 3, 243-247.
- [60] Peme, T.; Olasunkanmi, L.O.; Bahadur, I.; Adekunle, A.S.; Kabanda, M.M.; Ebenso, E.E. Adsorption and Corrosion Inhibition Studies of Some Selected Dyes as Corrosion Inhibitors for Mild Steel in Acidic Medium: Gravimetric, Electrochemical, Quantum Chemical Studies and Synergistic Effect with lodide lons. Molecules. 2015, 20, No. 9, 16004-16029.
- [61] Suarez-Hernandez, R.; Gonzalez-Rodriguez, Dominguez-Patiño, G.F.; Martinez-Villafañe, A. Use of Opuntia ficus Extract as a Corrosion Inhibitor for Carbon Steel in Acidic Media. Anti-Corros. Methods Mater. 2014, 61, No. 4, 224-231.
- [62] Ashassi-Sorkhabi, H.; Seifzadeh, D.; Hosseini, M.G. EN, EIS and Polarization Studies to Evaluate the Inhibition Effect of 3H-phenothiazin-3-one, 7-dimethylamin on Mild Steel Corrosion in 1 M HCl Solution. Corros. Sci. 2008, 50, No. 12, 3363-3370.
- [63] Osman, M.M.; Omar, A.M.A.; Al-Sabagh, A.M. Corrosion Inhibition of Benzyl Triethanol Ammonium Chloride and Its Ethoxylate on Steel in Sulphuric Acid Solution. Mater. Chem. Phys. 1997, 50, No. 3, 271-274.
- [64] Cabral, A.; Duarte, R.G.; Montemor, M.F.; Zheludkevich, M.L.; Ferreira, M.G.S. Analytical Characterisation and Corrosion Behaviour of bis-(triethoxysilylpropyl)tetrasulphide Pre-treated AA2024-T3. Corros. Sci. 2005, 47, No. 3, 869-881.
- [65] Cesiulis, H.; Tsyntsaru, N.; Ramanavicius, A.; Ragoisha, G. The Study of Thin Films by Electrochemical Impedance Spectroscopy. In Nanostructures and Thin Films for Multifunctional Applications; Tiginyanu, I., Topala, P., Ursaki, V., Eds.; Springer International: Cham, 2016; pp 3-42.

- [66] Somasundaran, P. Encyclopedia of Surface and Colloid Science, 2004 Update Supplement, CRC Press: New York, 2004.
- [67] Bommersbach, P.; Alemany-Dumont, C.; Millet, J.P.; Normand, B. Formation and Behaviour Study of an **Environment-Friendly** Corrosion Inhibitor by Electrochemical Methods. Electrochimica Acta. 2005, 51, No. 6, 1076-1084.
- [68] Gonçalves, R.S.; Azambuja, D.S.; Serpa Lucho, A.M. Electrochemical Studies of Propargyl Alcohol as Corrosion Inhibitor for Nickel, Copper, and Copper/ Nickel (55/45) Alloy. Corros. Sci. 2002, 44, No. 3, 467-479.
- [69] Ma, H.; Cheng, X.; Li, G.; Chen, S.; Quan, Z.; Zhao, S.; Niu, L. The Influence of Hydrogen Sulfide on Corrosion of Iron Under Different Conditions. Corros. Sci. 2000, 42, No. 10, 1669-1683.
- [70] Zulfareen, N.; Kannan, K.; Venugopal, T.; Gnanavel, S.: Synthesis, Characterization and Corrosion Inhibition Efficiency of N-(4-(Morpholinomethyl Carbamoyl Phenyl) Furan-2-Carboxamide for Brass in HCl Medium. *Arab. J. Chem.* **2016,** *9,* No. 1, 121–135.
- [71] Fouda, A.S.; Megahed, H.E.; Fouad, N.; Elbahrawi, N.M. Corrosion Inhibition of Carbon Steel in 1 M Hydrochloric Acid Solution by Aqueous Extract of Thevetia peruviana. J. Bio- Tribo-Corros. 2016, 2, No. 3, 1-13.
- [72] Oguzie, E.E. Corrosion Inhibition of Aluminium in Acidic and Alkaline Media by Sansevieria trifasciata Extract. Corros. Sci. 2007, 49, No. 3, 1527-1539.
- [73] Nwabanne, J.T.; Okafor, V.N. Adsorption Thermodynamics Study of the Inhibition of Corrosion of Mild Steel in H2SO4 Medium Using Vernonia amygdalina. J. Miner. Mater. Charact. Eng. 2012, 11, 885-890.
- [74] El-Sayed, A.-R.; Mohran, H.S.; Abd El-Lateef, H.M. The Inhibition Effect of 2,4,6-tris (2-pyridyl)-1,3,5-triazine on Corrosion of Tin, Indium and Tin-Indium Alloys in Hydrochloric Acid Solution. Corros. Sci. 2010, 52, No. 6, 1976-1984.
- [75] Shah, A.M.; Rahim, A.A.; Hamid, S.A.; Yahya, S. Green Inhibitors for Copper Corrosion by Mangrove Tannin. Int. J. Electrochem. Sci. 2013, 8, 2140-2153.
- [76] Honarvar Nazari, M.; Allahkaram, S.R.; Kermani, M.B. The Effects of Temperature and pH on the Characteristics of Corrosion Product in CO2 Corrosion of Grade X70 Steel. Mater. Des. 2010, 31, No. 7, 3559-3563.

- [77] Nazari, M.H.; Allahkaram, S.R. The Effect of Acetic Acid on the CO2 Corrosion of Grade X70 Steel. Mater. Des. 2010, 31, No. 9, 4290-4295.
- [78] Honarvar Nazari, M.; Ataie, A.; Seyyed Ebrahimi, S.A. Nano-Crystalline Barium Hexaferrite Powders Prepared by Mechanical Alloying Using Acetate Precursor. Key Eng. Mater. 2008, 368-372, 610-612.
- [79] Nazari, M.H.; Ataie, A.; Seyyed Ebrahimi, S.A. Effects of Processing Conditions on the Characteristics of Nano-Crystalline Barium Hexaferrite Prepared by Mechanical Alloying Method. Int. J. Mod. Phys. B 2008, 22, No. 18n19, 3127-3132.
- [80] Hunter, T. Why Nature Chose Phosphate to Modify Proteins. Philos. Trans. R. Soc. B Biol. Sci. 2012, 367, No. 1602, 2513-2516.
- [81] Wessling, B. Effective Corrosion Protection with the Organic Metal Polyaniline: Basic Principles and Recent Progress. In Electroactive Polymers for Corrosion Control, vol. 843, 0 vols., American Chemical Society, 2003; pp 34-73.
- [82] Surendranath, Y.; Kanan, M.W.; Nocera, D.G. Mechanistic Studies of the Oxygen Evolution Reaction by a Cobalt-Phosphate Catalyst at Neutral pH. J. Am. Chem. Soc. 2010, 132, No. 46, 16501-16509.
- [83] Kowsari, E.; Payami, M.; Amini, R.; Ramezanzadeh, B.; Javanbakht, M. Task-Specific Ionic Liquid as a New Green Inhibitor of Mild Steel Corrosion. Appl. Surf. Sci. **2014,** 289, 478-486.
- [84] Li, D.; Neumann, A.W. A Reformulation of the Equation of State for Interfacial Tensions. J. Colloid Interface Sci. 1990, 137, No. 1, 304-307.
- [85] Liu, D.; Zhao, W.; Liu, S.; Cen, Q.; Xue, Q. Comparative Tribological and Corrosion Resistance Properties of Composite Coatings Reinforced Functionalized Fullerene C60 and Graphene. Surf. Coat. Technol. 2016, 286, 354-364.
- [86] Malik, M.A.; Hashim, M.A.; Nabi, F.; AL-Thabaiti, S.A.; Khan, Z. Anti-corrosion Ability of Surfactants: A Review. Int. J. Electrochem. Sci. 2011, 6, 1927-1948.
- [87] Tang, Y.; Yang, X.; Yang, W.; Wan, R.; Chen, Y.; Yin, X. A Preliminary Investigation of Corrosion Inhibition of Mild Steel in 0.5 M H2SO4 by 2-amino-5-(n-pyridyl)-1,3,4-thiadiazole: Polarization, EIS and Molecular Dynamics Simulations. Corros. Sci. 2010, 52, No. 5, 1801–1808.